The Dynamics of Non-Upright Castor Wheels and Their Application for Pushing Wheelchairs from the Side.

Matto Leeuwis

Supervisor: Heike Vallery
Date started: September 2, 2020
Date finished: January 26, 2022

Technische Universiteit Delft

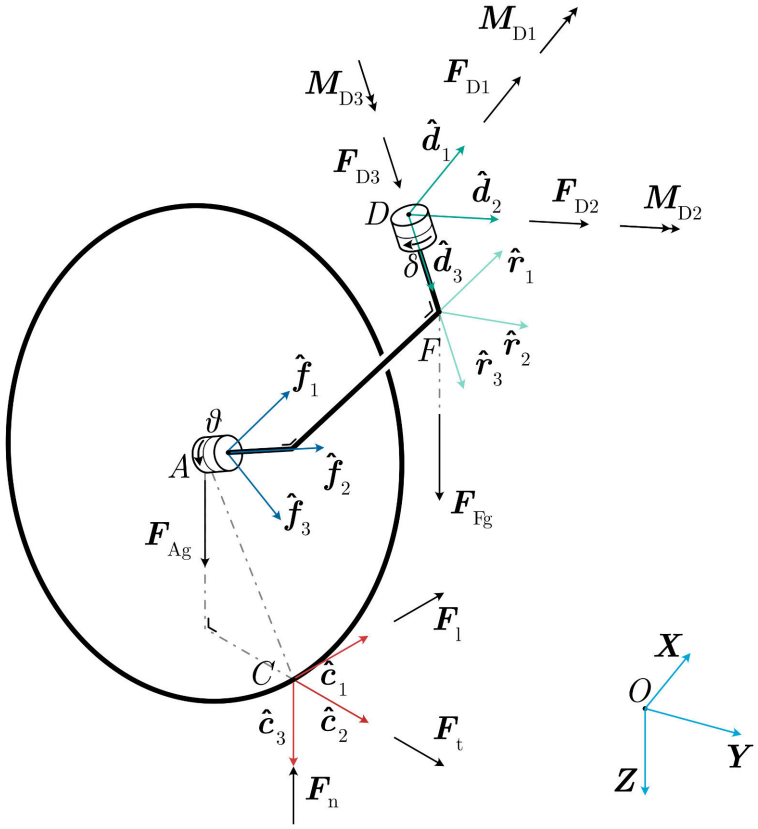

TU Delft

Erasmus MC
Universitair Medisch Centrum Rotterdam

The Dynamics of Non-upright Castor Wheels and Their Application for Pushing Wheelchairs from the Side.

by

Matto Leeuwis

to obtain the degree of Master of Science
at the Delft University of Technology,
to be defended publicly on January 26, 2022.

Student number: 4581067
Project duration: September 2, 2020 – January 26, 2022
Thesis committee: Prof. Dr. Ir. Heike Vallery (chair)
Prof. Dr. Dirk Jan Veeger
Dr. Barys Shyrokau

TU Delft

Erasmus MC
Universitair Medisch Centrum Rotterdam

M. Leeuwis, Delft, The Netherlands, compiled January 16, 2022

The Dynamics of Non-upright Castor Wheels and Their Application for Pushing Wheelchairs from the Side.

Matto Leeuwis

***Abstract*—Many wheelchair users, such as the elderly or children with Profound Intellectual and Multiple Disabilities (PIMD), rely on a caregiver to push them. The lack of eye contact between the wheelchair user and caregiver hinders communication and can even be dangerous, for example for children with epilepsy. Conventional wheelchairs place the caregiver behind the patient when pushing the wheelchair, but this position obstructs communication and makes it harder to assess the user's health.**

To facilitate face-to-face communication while walking, Lucy Bennett recently proposed a steering compensation method at BME2021 using a banked castor wheel to allow the caregiver to walk next to the wheelchair. This thesis contains a mathematical model for a castor wheel to determine how the three-dimensional orientation of the castor swivel axis and wheel spin axis, and external parameters such as rolling resistance affect the steering compensation. Both the Lagrange and virtual power methods are used to find the equations of motion of the castor wheel.

The steering effect was quantified as the moment generated by the wheelchair around its center of mass in the up direction. The cant angle of the castor wheel has the strongest steering effect. In the future, the developed mathematical model can be applied to calculate the influence of design variables to build a better prototype.

I. Introduction

The manual wheelchair plays an essential role in the life of many disabled people and caregivers, and usage of a manual wheelchair has a positive influence on the occupants' perceived ability to work or lead an active lifestyle when compared to an electrical wheelchair [1]. In this thesis, any person sitting in the wheelchair is referred to as the *occupant*, and any person who pushes the wheelchair while standing or walking as the *caregiver*. The caregiver or occupant can propel the wheelchair forward by applying a force on the handles or rims. However, if this propulsion is not symmetric, the wheelchair will turn to one side.

The propulsion can be assumed to be symmetric for healthy experienced wheelchair occupants [3], even though the dominant arm has a larger flexion strength [4]. People who have suffered a stroke have difficulty keeping a straight path due to the asymmetric forces of unilateral (one-sided) propulsion, which can be compounded by cognitive problems [2]. Stroke patients also desire the ability to move around independently rather than be pushed by a caregiver.

For children with Profound Intellectual and Multiple Disabilities (PIMD), face-to-face contact is crucial because they often can only communicate non-verbally [5]. It is also hard to assess the occupant's well-being and alertness from the position behind the wheelchair because the occupant and caregiver cannot make eye contact due to their respective positions.

It has been suggested to push the wheelchair from the side using a push bar to facilitate direct communication between the caregiver and occupant [6], [7]. However, if the caregiver applies a pure pushing force on the wheelchair from the side, a moment resulting from the push force will cause the wheelchair to turn. The caregiver can compensate by applying a free moment in the opposite direction, but this can lead to fatigue as muscle activation requires energy even if no mechanical work is done [8].

A solution was presented by Storch [9], where a clutch is used to couple the rear wheels. This solution only permits the wheelchair to drive in a straight trajectory, meaning that the caregiver does not have to apply the additional free moment.

To compensate for the asymmetric propulsion without limiting the trajectory of the wheelchair, Bennett [10] proposed a castor wheel with a non-vertical swivel axis. A *castor wheel* is defined as a wheel linked to a vehicle with a rigid connector, called the *castor fork*. The castor fork is connected to the vehicle with the castor stem, also called the *swivel axis*. Conventionally the swivel axis is perpendicular to the ground plane.

The castor wheel with a non-vertical swivel axis creates a preferred position for the wheel, and as a result, the wheelchair moves in a curve when a force is applied in the forward direction. Bennett performed a series of experiments to determine how the *cant* and *rake angle* influenced this curve. ISO 7176-26:2007 [11] defines the cant angle as the angle between the swivel axis and the vertical axis in the frontal plane. The rake angle is between the swivel axis and the vertical in the sagittal plane. Both angles are shown in Figure 1. In this study, the *wheel bank angle*, defined as the angle between the swivel axis and the wheel spin axis, is also considered and shown in Figure 1a.

Mathematical models for (castor) wheels with a rake angle have been developed for vehicles such as motorcycles, wave boards, and plane suspensions [12]–[14], but the cant angle is often ignored. A tilted steer axis was defined by de Falco et al. [15], but only results for the effect of the rake angle are shown. For wheelchairs specifically, all found literature assumes that the swivel axis is perpendicular to the ground plane.

This thesis aims to determine how a castor wheel can be modified to exert a force or moment on the wheelchair and validate the results of the experimental study conducted by Bennett. To do so, a set of design parameters is defined, and a dynamic model of the wheelchair with a single castor wheel is proposed. This model is used to determine the force and moment that the caregiver or occupant needs to provide to achieve the desired trajectory.

II. Problem definition

This section presents the parameters, geometry, and main assumptions. The forces responsible for the dynamics are

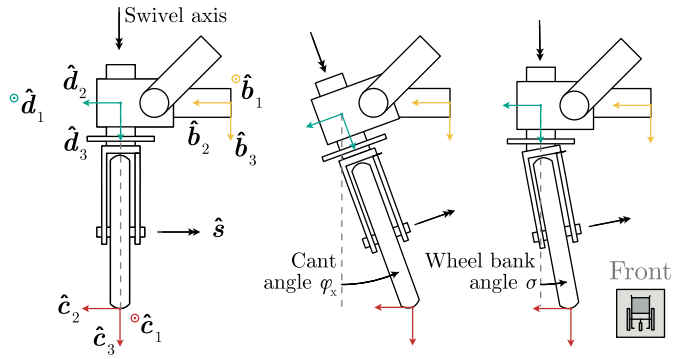

(a) Left: traditional castor wheel with swivel axis $\hat{\boldsymbol{d}}_3$ and wheel spin axis $\hat{\boldsymbol{s}}$. Middle: cant angle ϕ_x of swivel axis relative to the wheelchair. Right: wheel bank angle σ of wheel spin axis relative to swivel axis.

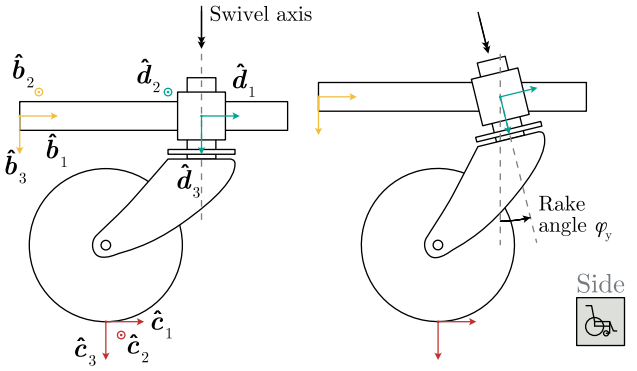

(b) Left: traditional castor wheel. Right: rake angle ψ_y of swivel axis relative to wheelchair.

Fig. 1: Overview of basic rotations for the swivel axis of the castor wheel.

defined, and the equations of motion of the wheelchair are established. In Sections III and IV the unknown forces in the equations of motion are derived.

A. Geometric description of the castor wheel and wheelchair

The parameters of the wheelchair can be split in multiple groups:

- Generalized coordinates: variables that describe the configuration of the wheelchair and change during simulation.
- Design parameters: values that can be chosen for the design.
- Environment parameters: values that cannot be chosen and are imposed on the system.
- Use variables: values that the caregiver and wheelchair occupant influence.

All parameters are constants, and the defined use variables can be changed during simulation. The generalized coordinates are used to describe the configuration of the wheelchair in Cartesian space. Due to kinematic constraints, not every combination of generalized coordinates is valid.

Consider a wheelchair with a single castor wheel at the front, named f1. The 'f' refers to a front wheel, and '1' is the

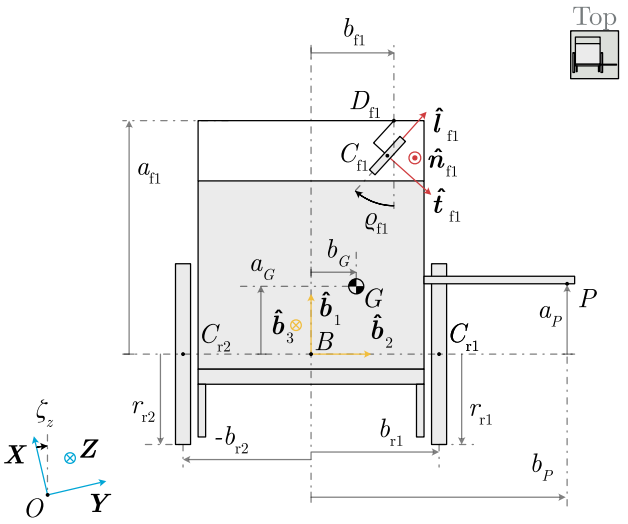

Fig. 2: Kinematic diagram with triad names and dimensions of the wheelchair.

index of the front wheel. There is only one front wheel in this case, so the index '1' is often omitted. In a similar manner the rear wheels are named $r1$ and $r2$ for the right and left wheel respectively. The radii of these wheels are r_{f1}, r_{r1}, and r_{r2} respectively. The kinematic diagram of the wheelchair is shown in Figure 2.

A *triad* is defined as a set of orthonormal unit vectors. The letter used for the names of these unit vectors is always the same as the lowercase letter for the triad. A body-fixed triad $\mathcal{B}$ consisting of unit vectors $\hat{\boldsymbol{b}}_1$, $\hat{\boldsymbol{b}}_2$, and $\hat{\boldsymbol{b}}_3$, is defined fixed to the wheelchair. Point B lies on the symmetry plane of the rear wheels. The location of points relative to point B is defined as a_i for dimensions in the $\hat{\boldsymbol{b}}_1$ direction, b_i for dimensions in the $\hat{\boldsymbol{b}}_2$ direction, and h_i for dimensions in the $\hat{\boldsymbol{b}}_3$ direction, where i is the name of the point. The rear wheels of the wheelchair are at positions b_{r1} and b_{r2} measured from point B. The connection between the wheelchair and the top plate of the castor wheel is named D_{f1}. The occupant is assumed to be rigidly attached to the wheelchair, and their combined center of mass is point G. An overview of these points and triads is shown in Figure 6a

The forces and moments on the body of the wheelchair are shown in the free-body diagram in Figure 3. The caregiver can push the wheelchair at the handle, which extends laterally. The point at which the pushing force F_P is applied is called P. In addition to the moment generated by the pushing force, the caregiver could also apply an additional free moment of magnitude M_P on the handle in the $\hat{\boldsymbol{b}}_3$ direction. Ideally, the wheelchair is designed such that M_P is zero. Therefore, this thesis aims to find design parameters such that the caregiver can push the wheelchair at point P without applying an additional free moment M_P.

The castor wheel can be modeled as a wheel and a castor fork. The kinematic diagram of the castor wheel is shown in Figure 6b. To clarify the order of the rotations, a *cans-in-series* representation [16] is given in Figure 6c. Each can represents

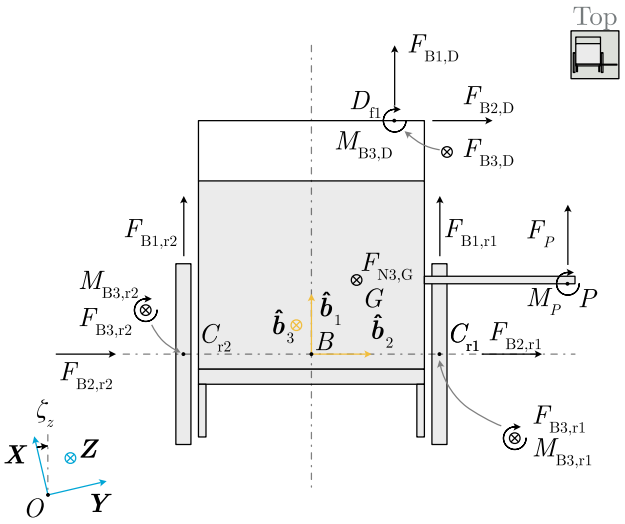

Fig. 3: Free-body diagram of the wheelchair.

a rotation with the angle name printed next to it. Some angles such as σ are constant design parameters, while others such as δ can vary over time.

The wheel is modeled as a flat disk and can only rotate relative to the castor fork around spin axis $\hat{\boldsymbol{s}}$ with angle θ. The fork can only rotate relative to the vehicle around the swivel axis with angle δ. All dimensions and the rotations θ and δ are shown in Figure 6b. A triad $\mathcal{D}$ is defined along the swivel axis to determine the rotation of the swivel axis with respect to the wheelchair. This triad can be rotated with respect to the wheelchair with cant angle ϕ_x and rake angle[1] ϕ_y.

Triads $\mathcal{R}$ and $\mathcal{F}$ are both fixed to the castor fork. Triad $\mathcal{R}$ is rotated with swivel angle δ with respect to triad $\mathcal{D}$. The orientation of the wheel spin axis $\hat{\boldsymbol{s}}$ with respect to triad $\mathcal{R}$ is given by wheel bank angle σ, which is a rotation around $\hat{\boldsymbol{r}}_1$. The location of the center of the wheel with respect to point F is given by L_{ex} and L_{ey}, also referred to as the castor trail. The full equations for the kinematics of the castor wheel can be found in Appendix A.

B. Generalized coordinates

The configuration of the wheelchair chassis can be described using the location and orientation of the body. The X, Y, and Z location of point B are defined as x_B, y_B, and z_B. The yaw, pitch, and roll angles with respect to the inertial coordinate system are ζ_z, ζ_y, and ζ_x respectively. One additional degree of freedom is added for the rotation of each rear wheel, named θ_{ri}. Each castor wheel of the wheelchair adds two additional degrees of freedom: one for swivel angle δ_{fi} and one for the rotation of the wheel θ_{fi}. Therefore a wheelchair with one front and two rear wheels can be described with the following generalized coordinate vector[2].

$$\boldsymbol{q}_{\text{wc}} = \begin{pmatrix} x_B & y_B & z_B & \zeta_x & \zeta_y & \zeta_z & \theta_{\text{r1}} & \theta_{\text{r2}} & \theta_{\text{f1}} & \delta_{\text{f1}} \end{pmatrix}^{\text{T}} \tag{1}$$

Some of these generalized coordinates can be removed or replaced if the following assumptions are made.

Assumption 1: The ground plane is flat and perpendicular to gravity.

Assumption 2: The wheel is always in contact with the ground and never slips, regardless of the reaction forces.

Assumption 3: The pitch angle ζ_y of the wheelchair is small, and does not contribute to lateral and longitudinal displacements of any points. These displacements are shown in Figure 4. Proof is shown in Appendix D.

Assumption 4: The height of point D_{f1} is a linear function of the pitch angle ζ_y, and can be substituted by a new variable z_D. Proof is shown in Appendix D.

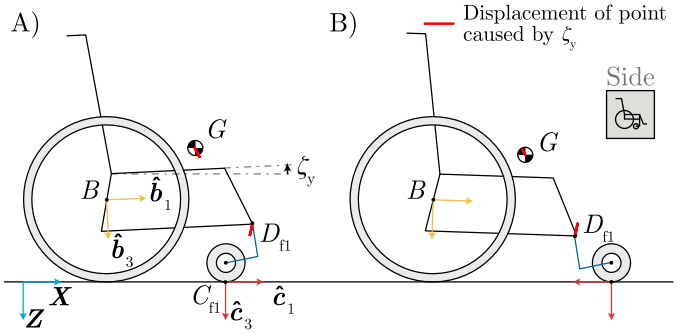

Fig. 4: Displacement of points G and D_{f1} caused by the pitch angle ζ_y of the wheelchair. Pitch angle is a function of the castor wheel swivel angle δ. A) smallest possible pitch angle for a castor wheel with pure rake. B) largest possible pitch angle for a castor wheel with pure rake.

Using these assumptions, the generalized coordinate vector simplifies to Equation 2.

$$\boldsymbol{q} = \begin{pmatrix} x_B & y_B & \zeta_z & \theta & \delta & z_D \end{pmatrix}^{\text{T}} \tag{2}$$

The wheelchair with these generalized coordinates has a constant pitch angle and instead only permits change in the height of point D_{f1}. The inertia of the vertical translation of the center of mass of the wheelchair chassis due to a change in swivel angle δ is ignored with this description. The vertical load on the castor is modeled as a constant-force spring. The compressive force in this spring is the vertical load $F_{\text{B3,D}}$ on the castor wheel. The constant-force spring representation is shown in Figure 5.

C. Equations of motion of the wheelchair

The equations of motion of the wheelchair can be determined using the free-body diagram in Figure 3. The caregiver provides a pushing force of F_P at point P, which is at a distance of b_P from point B. In addition, the caregiver can apply a free moment M_P on the push bar.

[1]Names for cant and rake angle are determined by ISO 7176-26:2007(en) [11]

[2]This is a compact way of writing the generalized coordinates, but it is not a proper vector. Most vector properties do not apply to $\boldsymbol{q}$ because its elements can have different units, and its basis is usually not orthogonal.

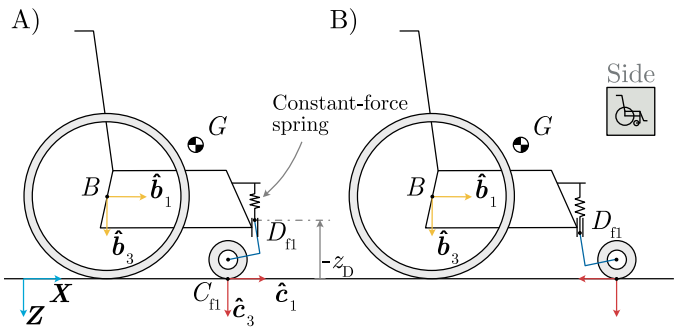

Fig. 5: Side view of the wheelchair with the generalized coordinates from Equation 2 with the same swivel angles δ as Figure 4. With this description the pitch angle ζ_y is constant, but the castor wheel can still swivel due to the constant-force spring.

The following assumptions are made to find the equations of motion:

Assumption 5: Both rear wheels always have equal rolling resistance. This assumption is only valid if the connection between the wheelchair and castor D, and the center of mass G lie close to or in the symmetry plane of the wheelchair.

Assumption 6: The center of mass G of the wheelchair lies in the symmetry plane of the wheelchair, so $b_G = 0$.

Assumption 7: The wheels have no turning resistance, so no moment is transmitted at contact in direction $\hat{\boldsymbol{n}}$.

Assumption 8: There is no friction in the bearings, so $\boldsymbol{M}_{\mathrm{D3}} = \boldsymbol{0}$.

Assumption 9: The fraction of weight supported by the front wheels P_f relative to the total weight is constant over time. Proof given in Appendix E.

Assumption 10: The rolling resistance coefficient only depends on the floor type, wheel type, and wheel radius.

Assumption 11: The caregiver applies on point P a force F_P in the forward $\hat{\boldsymbol{b}}_1$ direction, and a free moment M_P in the down $\hat{\boldsymbol{b}}_3$ direction. There are no components of the force and moment in other directions.

In Appendix E the derivation based on these assumption is shown (Apppendix E Equation A.109 to A.111). The equations of motion are

$$m_G \ddot{\boldsymbol{r}}_G \cdot \hat{\boldsymbol{b}}_1 = F_{\mathrm{B1,D}} + \sum_{i=1}^{2} F_{\mathrm{B1,ri}} + F_{\mathrm{P}}, \tag{3}$$

$$m_G \ddot{\boldsymbol{r}}_G \cdot \hat{\boldsymbol{b}}_2 = F_{\mathrm{B2,D}} + \sum_{i=1}^{2} F_{\mathrm{B2,ri}}, \tag{4}$$

$$\begin{aligned} \ddot{\zeta}_z I_{\mathrm{B3,G}} = M_{\mathrm{P}} - b_P F_P + M_{\mathrm{B3,D}} - b_{\mathrm{fl}} F_{\mathrm{B1,D}} \\ +(a_{\mathrm{fl}} - a_G) F_{\mathrm{B2,D}} - \sum_{i=1}^{2} a_G F_{\mathrm{B2,ri}}, \end{aligned} \tag{5}$$

where

F_P is the applied force by the caregiver,
M_P is the applied free moment by the caregiver,
F_{Bj} is a force in direction $\hat{\boldsymbol{b}}_{\mathrm{j}}$,
$M_{\mathrm{Bj,B}}$ is a moment in direction $\hat{\boldsymbol{b}}_{\mathrm{j}}$ calculated around point B,
$F_{\mathrm{Bj,D}}$ is a force in direction $\hat{\boldsymbol{b}}_{\mathrm{j}}$ on point D,
$F_{\mathrm{Bj,ri}}$ is a force in direction $\hat{\boldsymbol{b}}_{\mathrm{j}}$ on rear wheel i,
$\ddot{\boldsymbol{r}}_G$ is the acceleration of the center of mass G,
$I_{\mathrm{B3,G}}$ is the mass moment of inertia of the wheelchair and occupant around G in the $\hat{\boldsymbol{b}}_3$ direction.

The roll resistance and forces on the castor connection D in the equation of motion can be written as a function of the vertical load on the wheels. Assumption 9 implies that the vertical load on the rear and front wheels is constant over time. The vertical forces on front and rear wheels are equal to

$$F_{\mathrm{B3,D}} = P_f m_{\mathrm{wc}} g, \tag{6}$$

$$F_{\mathrm{B3,ri}} = \frac{P_r}{2} m_{\mathrm{wc}} g, \tag{7}$$

where

P_f is the fraction of the total weight that is supported by the front wheels,
P_r is the fraction of the total weight that is supported by the rear wheels such that $P_r = 1 - P_f$,
g is the gravity constant of $9.81\,\mathrm{m/s^2}$,
m_{wc} is the total weight of the wheelchair and occupant.

The location of the center of mass a_G can be written as a function of P_f. Johnson and Aylor [17] approximated P_f as $1/3$. The longitudinal location of the center of mass as a function of P_f is equal to

$$a_G = a_{\mathrm{fl}} P_f. \tag{8}$$

The rolling resistance can be approximated with a constant coefficient of rolling resistance $f_{r,r}$ for the rear wheels, and $f_{r,f}$ for the front wheels. This coefficient depends on the floor type, wheel type, wheel radius, velocity, and tire pressure [18]. Sauret et al. [19] determined that velocity and tire pressure contribute less than $5\,\%$ to the roll resistance of the wheelchair, so these are neglected in Assumption 10. The values of the roll resistance coefficients are shown in Table I.

Wheel	Type	Radius	Roll resistance coefficient	
			Hard smooth surface	Carpet
Castor wheel	Standard	10 cm	0.02	0.035
Rear wheel	Pneumatic	28 cm	0.005	0.015

TABLE I: Roll resistance coefficients for the front and rear wheels on two different surface types. Values from work by Sauret et al. [19].

The rolling resistance of the rear wheels combined is

$$F_{\mathrm{B1,ri}} = \mathrm{sgn}\left(\dot{\theta}_{\mathrm{ri}}\right) F_{\mathrm{B3,ri}}\, f_{\mathrm{r,r}} = \mathrm{sgn}\left(\dot{\theta}_{\mathrm{ri}}\right) m_{\mathrm{wc}}\, g\, \frac{P_r}{2}\, f_{\mathrm{r,r}}, \tag{9}$$

and the rolling resistance on the castor wheel in the direction of unit vector $\hat{\boldsymbol{l}}$ is

$$F_l = \mathrm{sgn}\left(\dot{\theta}_{\mathrm{fl}}\right) F_{\mathrm{B3,D}}\, f_{\mathrm{r,f}} = \mathrm{sgn}\left(\dot{\theta}_{\mathrm{fl}}\right) m_{\mathrm{wc}}\, g\, P_f\, f_{\mathrm{r,f}}, \tag{10}$$

where

F_l is the force on the castor in the longitudinal contact direction $\hat{\boldsymbol{l}}$,
$f_{\mathrm{r,f}}$ is the rolling resistance factor of the front wheel,

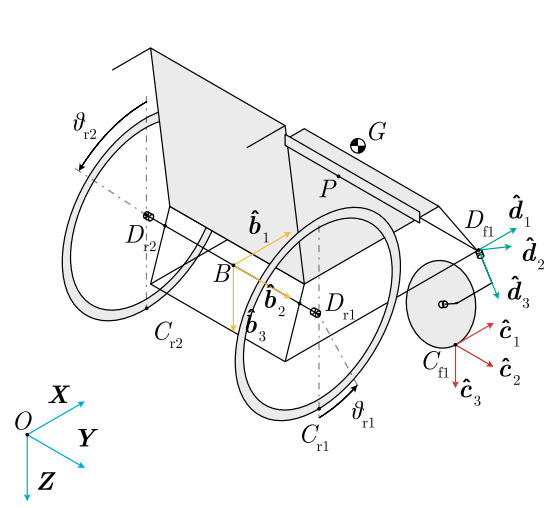

(a) Overview of important points and triads on the wheelchair.

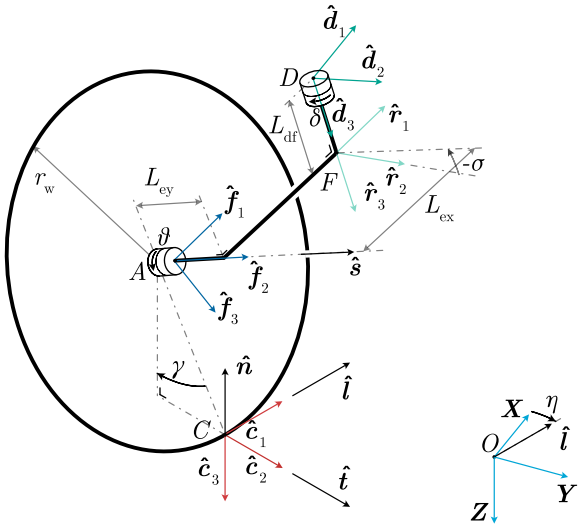

(b) Kinematic diagram of the castor wheel.

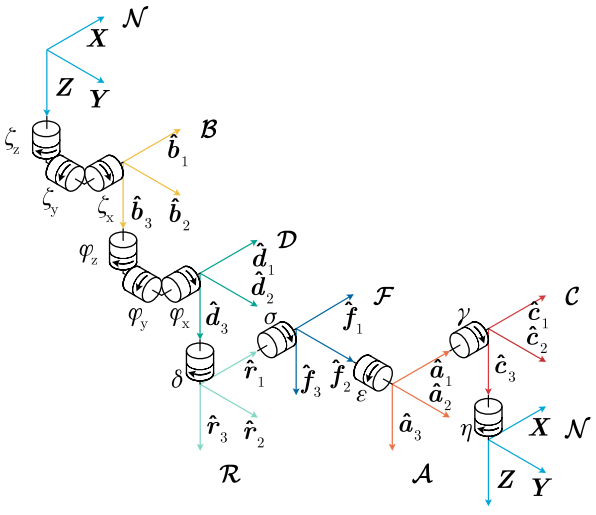

(c) Cans-in-series [16] representation of the used triads. The arrow on each can indicates the direction of a positive rotation when the triad on the left hand side is grounded.

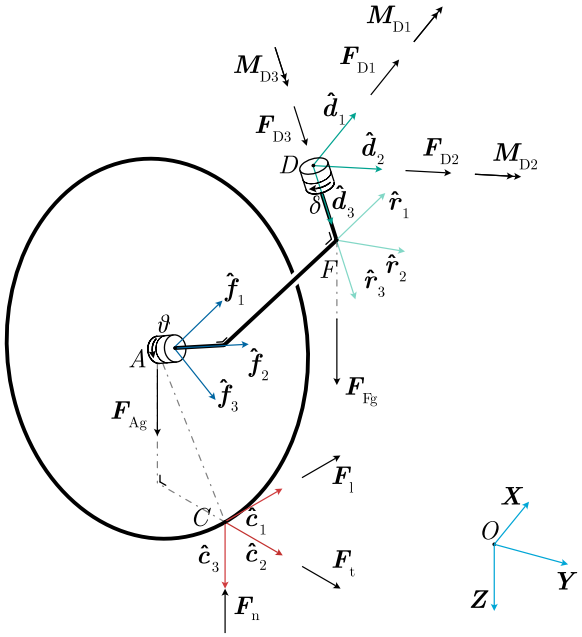

(d) Free-body diagram of the castor wheel.

Fig. 6: Overview of kinematics and dynamics of the wheelchair and castor wheel.

$f_{\mathrm{r,r}}$ is the rolling resistance factor of the rear wheel.

The roll resistance on the castor wheel F_l does not appear in the equations of motion explicitly, but is required to find the forces on the castor connection D.

D. Preferred orientation of the castor wheel

The presence of a cant and/or rake angle will introduce a preferred rotation of the castor wheel. The cant and rake angle ϕ_x and ϕ_y of the swivel axis will determine in what direction the wheel will rotate and settle.

Mathematically the preferred position is the swivel angle δ where the potential energy is smallest. This means that the height z_D of point D is closest to the ground plane. In this configuration the wheelchair is in static equilibrium. If the swivel axis coincides with the wheel plane ($\sigma = 0, L_{\mathrm{ey}} = 0$, see Figure 6b), then the preferred direction is the projection of $\hat{\boldsymbol{d}}_3$ onto the ground plane.

$$\hat{\boldsymbol{l}}_{\mathrm{pref}} = -\frac{\hat{\boldsymbol{d}}_3 - (\hat{\boldsymbol{d}}_3 \cdot \hat{\boldsymbol{n}})\hat{\boldsymbol{n}}}{\left\|\hat{\boldsymbol{d}}_3 - (\hat{\boldsymbol{d}}_3 \cdot \hat{\boldsymbol{n}})\hat{\boldsymbol{n}}\right\|} \tag{11}$$

where

$\hat{\boldsymbol{l}}_{\mathrm{pref}}$ is the direction of the longitudinal contact of the castor wheel $\hat{\boldsymbol{l}}$ where the wheelchair is in a stable static equilibrium,

$\hat{\boldsymbol{n}}$ is the normal vector up out of the ground plane,

$\hat{\boldsymbol{d}}_3$ is the direction of the swivel axis.

III. Steady-state approximation of the reaction forces

In this section, a steady-state approximation is made for the force and moment applied by the caregiver. This solution is only valid if the wheelchair moves in uniform circular motion, and can be used to select design parameters for the wheelchair and castor wheel.

A. Equations of motion in uniform circular motion

In uniform circular motion, the forward velocity of B and angular velocity of the wheelchair chassis are constant. Point B is located between the two rear wheels, meaning that it cannot have a velocity in the lateral $\hat{\boldsymbol{b}}_2$ direction due to the no slip condition of the rear wheels.

Since the caregiver can choose what force and moment to apply, we can make the following assumption:

Assumption 12: The caregiver applies a force or moment such that the motion of the body of the wheelchair is uniform circular motion. The forward velocity and yaw rate of the wheelchair are constant over time.

The turn radius r_{turn} of the uniform circular motion is defined positive for right turns, and is measured from point B. The yaw rate $\dot{\zeta}_z$ for uniform circular motion of the wheelchair is calculated with

$$\dot{\zeta}_z = \frac{v_{\mathrm{wc}}}{r_{\mathrm{turn}}}, \tag{12}$$

where

$\dot{\zeta}_z$ is the time derivative of the yaw angle ζ_z of the wheelchair,

v_{wc} is the forward velocity of the wheelchair,

r_{turn} is the turn radius of the wheelchair.

Even if v_{wc} and r_{turn} are constant, the acceleration of the center of mass $\ddot{\boldsymbol{r}}_G$ in both the forward and lateral direction is not zero. In multiple studies [20]–[22] this acceleration is ignored. However, even on low velocities, it can have a significant contribution [17], [23]. Sonenblum et al. [24] determined that the daily average speed of wheelchair users falls within a range of $0.5\,\mathrm{m/s}$ to $0.8\,\mathrm{m/s}$.

The acceleration of point B is given by

$${}^{\mathcal{B}}\ddot{\boldsymbol{r}}_B = \begin{pmatrix} \dot{v}_{\mathrm{wc}} \\ r_{\mathrm{turn}}\dot{\zeta}_z^2 \\ 0 \end{pmatrix}. \tag{13}$$

In uniform circular motion, the component $\dot{v}_{\mathrm{wc}}$ is zero because the forward velocity is constant. The acceleration of the center of mass G is found by adding the relative acceleration of G with respect to B. Recall that b_G was assumed zero in Assumption 6, otherwise an extra term is required in the $\hat{\boldsymbol{b}}_2$ direction.

$${}^{\mathcal{B}}\ddot{\boldsymbol{r}}_G = {}^{\mathcal{B}}\ddot{\boldsymbol{r}}_B + {}^{\mathcal{B}}\ddot{\boldsymbol{r}}_{G/B} = \begin{pmatrix} \dot{v}_{\mathrm{wc}} - a_G\dot{\zeta}_z^2 \\ r_{\mathrm{turn}}\dot{\zeta}_z^2 \\ 0 \end{pmatrix} \tag{14}$$

The pushing force of the caregiver F_P can be found by substituting Equation 14 in Newton's second law in the $\boldsymbol{b}_1$ direction, as given in Equation 3.

$$F_{\mathrm{P}} = -m_{\mathrm{wc}}a_G\dot{\zeta}_z^2 - F_{\mathrm{B1,D}} - \sum_{i=1}^{2} F_{\mathrm{B1,ri}} \tag{15}$$

In a case where the wheelchair drives in a straight line ($\rho = 0$), the force by the caregiver is given by

$$F_{\mathrm{P}}|_{\rho=0} = m_{\mathrm{wc}}g(P_f f_{r,r} + P_r f_{r,f}). \tag{16}$$

The sum of lateral forces on the rear wheels of the wheelchair in uniform circular can be found by substituting Equation 14 in Newton's second law in the $\boldsymbol{b}_2$ direction, as given in Equation 4.

$$\sum_{i=1}^{2} F_{\mathrm{B2,ri}} = m_{\mathrm{wc}}r_{\mathrm{turn}}\dot{\zeta}_z^2 - F_{\mathrm{B2,D}}. \tag{17}$$

The free moment M_P that the caregiver has to apply depends on where on the push bar the wheelchair is pushed. By substituting Equation 17 in Equation 5, the contribution of the lateral forces on the rear wheels can be replaced.

$$\begin{aligned} \ddot{\zeta}_z^2 I_{\mathrm{G,z}} = 0 = M_{\mathrm{P}} - b_{\mathrm{P}}F_{\mathrm{P}} + M_{\mathrm{B3,D}} - b_{\mathrm{f1}}F_{\mathrm{B1,D}} \\ + a_{\mathrm{f1}}F_{\mathrm{B2,D}} - m_{\mathrm{wc}}\dot{\zeta}_z^2 r_{\mathrm{turn}}a_G \end{aligned} \tag{18}$$

Equation 18 can be split between M'_P and $M'_{\neg P}$ as

$$M'_P + M'_{\neg P} = 0 \tag{19}$$

where

M'_P is the contribution of the caregiver to the sum of moments,

$M'_{\neg P}$ is the sum of all other moments that are not generated by the user, such as the moment generated by the castor wheel.

The contribution of the caregiver to Equation 18 is

$$M'_P = M_\mathrm{P} - b_\mathrm{P} F_\mathrm{P}, \tag{20}$$

and all other moments are equal to

$$M'_{\neg P} = M_{\mathrm{B3,D}} - b_{\mathrm{f1}} F_{\mathrm{B1,D}} + a_{\mathrm{f1}} F_{\mathrm{B2,D}} - m_\mathrm{wc} \dot{\zeta}_z^2 r_\mathrm{turn} a_G. \tag{21}$$

To maintain uniform circular motion, the caregiver must choose the force F_P and moment M_P such that the contribution by the caregiver M'_P is the exact opposite of $M'_{\neg P}$.

B. Push location on the handlebar

The caregiver can choose the location b_P on the push bar, and change it while pushing. However, the ideal point might not lie on the push bar, meaning that the caregiver must still apply a free moment to reach the desired value of M'_P. The smallest distance to push is chosen to be above the rear wheel, so $b_{P\min} = b_{\mathrm{r1}}$, and the largest distance is determined by the choice of the length of the push bar.

If we assume that the moment M_P is not required to reach equilibrium, then the ideal push position b_P is calculated as

$$b_\mathrm{P}|_{M_P=0} = \frac{M'_{\neg P}}{F_\mathrm{P}}. \tag{22}$$

To find $M'_{\neg P}$ and F_P, the lateral and longitudinal force on castor connection D must be determined. The longitudinal contact force F_l is given in Equation 10, but the lateral contact force F_t is still unknown.

C. Steady-state approximation of lateral force on the castor

In steady-state, the first and second time derivative of the swivel angle δ equal zero. The following set of assumptions are used in addition to the ones defined in section II

Assumption 13: The wheelchair has converged to a steady-state. This means that the body moves in uniform circular motion, and in addition that the swivel angle δ does not change over time.

Assumption 14: The small-angle approximation can be applied to ϕ_x, ϕ_y and σ.

Assumption 15: The weight of the components of the castor wheel is negligible compared to the weight of the wheelchair and occupant.

Since there is no friction in the bearings and the castor is massless, the moment acting on the castor fork around the swivel axis must equal zero.

$$M_{D3} = \boldsymbol{M}_D \cdot \hat{\boldsymbol{d}}_3 = 0, \tag{23}$$

where

- M_{D3} is the magnitude of the moment around the swivel axis $\boldsymbol{M}_{\mathrm{D3}}$, drawn in Figure 6d,
- $\boldsymbol{M}_D$ is the reaction moment vector around point D on the castor fork, equal to $\boldsymbol{M}_{\mathrm{D1}} + \boldsymbol{M}_{\mathrm{D2}} + \boldsymbol{M}_{\mathrm{D3}}$,
- $\hat{\boldsymbol{d}}_3$ is the unit vector in the direction of the swivel axis.

At contact point C the reaction forces are parametrized as

$${}^{\mathcal{C}}\boldsymbol{F}_\mathrm{C} = \begin{pmatrix} F_l \\ F_t \\ -F_n \end{pmatrix}, \tag{24}$$

where

- F_t is the lateral force on the castor wheel along unit vector $\hat{\boldsymbol{t}}$,
- F_l is the longitudinal force on the castor wheel along unit vector $\hat{\boldsymbol{l}}$,
- F_n is the normal force on the castor wheel along unit vector $\hat{\boldsymbol{n}}$.

In Appendix B Equation 23 is solved using the kinematics from Appendix A. This results in the following equation for the lateral force on the castor wheel F_t (Appendix B Equation A.53)

$$F_t = \frac{A_1 \left(\phi_y F_n + F_l \cos\left(\delta\right)\right) + B_1 \left(\phi_x F_n - F_l \sin\left(\delta\right)\right)}{B_1 \cos\left(\delta\right) + A_1 \sin\left(\delta\right)}, \tag{25}$$

where

$$\begin{aligned} A_1 = {} & L_\mathrm{ex} \sin\left(\delta\right) - L_\mathrm{ey} \cos\left(\delta\right) + r_w \sigma \cos\left(\delta\right) \\ & + r_w \sin\left(\delta\right) \left(\phi_y \cos\left(\delta\right) - \phi_x \sin\left(\delta\right)\right), \end{aligned} \tag{26}$$

$$\begin{aligned} B_1 = {} & L_\mathrm{ex} \cos\left(\delta\right) + L_\mathrm{ey} \sin\left(\delta\right) - r_w \sigma \sin\left(\delta\right) \\ & + r_w \cos\left(\delta\right) \left(\phi_y \cos\left(\delta\right) - \phi_x \sin\left(\delta\right)\right). \end{aligned} \tag{27}$$

The force vector ${}^{\mathcal{C}}\boldsymbol{F}_\mathrm{C}$ can be converted to the $\mathcal{B}$ triad using rotation matrix ${}^{\mathcal{C}}\mathbf{R}_{\mathcal{B}}$. Because of the small-angle approximation, the swivel angle δ is roughly equal to steer angle ρ (Appendix B Equation A.57). Therefore the rotation matrix ${}^{\mathcal{C}}\mathbf{R}_{\mathcal{B}}$ can be simplified to

$${}^{\mathcal{B}}\mathbf{R}_{\mathcal{C}} = \begin{pmatrix} \cos\left(\delta\right) & -\sin\left(\delta\right) & 0 \\ \sin\left(\delta\right) & \cos\left(\delta\right) & 0 \\ 0 & 0 & 1 \end{pmatrix}. \tag{28}$$

The force F_C projected on the directions of the $\mathcal{B}$ triad is

$${}^{\mathcal{B}}\boldsymbol{F}_\mathrm{C} = {}^{\mathcal{B}}\mathbf{R}_{\mathcal{C}} {}^{\mathcal{C}}\boldsymbol{F}_\mathrm{C} = \begin{pmatrix} F_l \cos\left(\delta\right) - F_t \sin\left(\delta\right) \\ F_t \cos\left(\delta\right) + F_l \sin\left(\delta\right) \\ -F_n \end{pmatrix}. \tag{29}$$

From this equation the elements of the force vector drawn in Figure 3 can be derived, given the fact that the castor wheel is in massless and in steady-state. This means that the reaction forces at C are opposite of those at D.

$$F_{\mathrm{B1,D}} = F_l \cos\left(\delta\right) - F_t \sin\left(\delta\right) \tag{30}$$

$$F_{\mathrm{B2,D}} = F_t \cos\left(\delta\right) + F_l \sin\left(\delta\right) \tag{31}$$

The free moment around point D in the $\hat{\boldsymbol{b}}_3$ direction depends linearly on both the lateral force F_t and the longitudinal force F_l and is equal to (Appendix B Equation A.67)

$$M_{\mathrm{B3,D}} = F_t A_2 + F_l B_2, \tag{32}$$

where

$$A_2 = -L_\mathrm{ex} + L_\mathrm{df} \phi_y \cos\left(\delta\right) - L_\mathrm{df} \phi_x \sin\left(\delta\right), \tag{33}$$

$$\begin{aligned} B_2 = {} & r_w \sigma - L_\mathrm{ey} + \phi_x r_w \cos\left(\delta\right) + \phi_y r_w \sin\left(\delta\right) \\ & + L_\mathrm{df} \phi_x \cos\left(\delta\right) + L_\mathrm{df} \phi_y \sin\left(\delta\right). \end{aligned} \tag{34}$$

The term A_2 is generally larger than B_2, since the longitudinal castor trail L_ex tends to be larger than the lateral castor trail L_ey.

D. Special cases for the steady-state approximation

The wheelchair moves in a straight line if ρ is zero. One case where this is true is if swivel angle δ and rake angle ϕ_y both are zero. For this straight-line path, Equations 25 and 32 simplify to

$$F_t|_{\delta=0 \wedge \phi_y=0} = -\frac{F_l\ (L_{\mathrm{ey}} - r_w\,\sigma) - L_{\mathrm{ex}}\,\phi_x\,F_n}{L_{\mathrm{ex}}} \tag{35}$$

and

$$\begin{aligned} &M_{\mathrm{B3,D}}|_{\delta=0 \wedge \phi_y=0} = \\ &F_l\,(L_{\mathrm{df}}\,\phi_x - L_{\mathrm{ey}} + \phi_x\,r_w + r_w\,\sigma) - F_t\,L_{\mathrm{ex}}. \end{aligned} \tag{36}$$

The influence of F_l on F_t can then be ignored by designing the lateral trail L_{ey} and wheel bank angle σ such that

$$L_{\mathrm{ey}} - r_w\,\sigma = 0. \tag{37}$$

A change in height between C and D can be prevented by choosing the length of the castor stem L_{df} such that

$$-L_{\mathrm{df}} + r_w + L_{\mathrm{ey}}\sigma = \mathrm{Constant}. \tag{38}$$

Equation 37 and 38 can be used to design a castor wheel such that the influence of F_l on F_t is small.

IV. Multibody simulation

A three dimensional multibody model is established to determine the reaction forces of the castor and the required forces and moments by the caregiver. First, the constraints and generalized coordinates are established, then both the Lagrange and TMT methods are used to derive the equations of motion. The model is used to validate the steady-state assumption made in section III and can be used to simulate trajectories that are not steady-state.

A. Kinematic constraints

At least four constraint equations on the generalized coordinates $\boldsymbol{q}$ and their derivatives are required. The first constraint is holonomic and ensures that point C is always in contact with the ground plane.

$$C_{\mathrm{C\_normal}} = \boldsymbol{r}_{C/O} \cdot \hat{\boldsymbol{n}} = 0 \tag{39}$$

Two nonholonomic constraints are used to prevent slip of the castor wheel in the lateral and longitudinal directions:

$$C_{\mathrm{C\_longitudinal}} = \dot{\boldsymbol{r}}_{C/O} \cdot \hat{\boldsymbol{l}} - \dot{\theta} r_w = 0, \tag{40}$$

$$C_{\mathrm{C\_tangent}} = \dot{\boldsymbol{r}}_{C/O} \cdot \hat{\boldsymbol{t}} = 0. \tag{41}$$

One nonholonomic constraint prevents lateral slip at the rear wheels. Since the rotation of the rear wheels is not present in the state vector $\boldsymbol{q}$, no constraint is required for the longitudinal direction.

$$C_{\mathrm{B\_tangent}} = \dot{\boldsymbol{r}}_{B/O} \cdot \hat{\boldsymbol{b}}_2 = 0 \tag{42}$$

After applying these constraints, five degrees of freedom are left in configuration space and two in velocity space. If uniform circular motion is assumed (Assumption 12), the caregiver can be modeled as a constraint on the forward and angular velocity. These constraints encode the force and moment that the caregiver needs to apply to keep the (angular) velocity of the wheelchair constant.

$$C_{\mathrm{B\_fixed\_velocity}} = \dot{\boldsymbol{r}}_{B/O} \cdot \hat{\boldsymbol{b}}_1 - v_{\mathrm{wc}} \quad = 0 \tag{43}$$

$$C_{\mathrm{B\_fixed\_rotation}} = \dot{\zeta}_z - \frac{v_{\mathrm{wc}}}{r_{\mathrm{turn}}} \quad = 0 \tag{44}$$

where

- r_{turn} is the constant turn radius of the wheelchair as measured from point B. A positive turn radius corresponds to a right turn.
- v_{wc} is the constant forward velocity of point B.

When these additional constraints are used, the system has zero degrees of freedom in velocity space. Therefore the motion is always the same regardless of forces once initial conditions and parameters have been chosen.

B. External forces and moments

Forces on the system can be split in three groups: constraint forces, conservative forces F_{cons} and forces that can be non-conservative: F_{ncons}. Constraint forces are governed by the Lagrange multipliers of the respective constraint, and are not included in the applied forces and moments. Any force which might be non-conservative must be included in F_{ncons}. The conservative non-constraint forces are gravity on the wheelchair, castor fork, and castor wheel. The non-conservative forces are rolling resistance on the front and rear wheels. The equations for the conservative forces are

$$F_{\mathrm{N3,G}} = m_{\mathrm{wc}} g, \tag{45}$$

$$F_{\mathrm{Fg}} = m_f g, \tag{46}$$

$$F_{\mathrm{Ag}} = m_w g, \tag{47}$$

where

- $F_{\mathrm{N3,G}}$ is the gravitational force on the center of mass of the wheelchair frame and occupant combined, point G,
- F_{Fg} is the gravitational force on the center of mass of the castor fork, assumed to be point F,
- F_{Ag} is the gravitational force on the center of mass of the wheel, point A,
- m_f is the mass of the castor fork,
- m_w is the mass of the castor wheel (without fork).

The equations for the roll resistance forces are given in Equation 9 and 10. The contributions of the caregiver M'_P are modelled as constraints, so they are included in neither F_{cons} nor F_{ncons}.

C. Derivation of equations of motion

The equations of motion are derived using both the Lagrange method and the TMT method [25]. The full derivation can be found in Appendix F. Both methods yield a system in the form of

$$\begin{pmatrix} \bar{\mathbf{M}} & \mathbf{C}_q^{\mathrm{T}} \\ \mathbf{C}_q & \mathbf{0} \end{pmatrix} \begin{pmatrix} \ddot{\boldsymbol{q}} \\ \boldsymbol{\lambda} \end{pmatrix} = \begin{pmatrix} \boldsymbol{f} \\ \mathbf{C}_{qq}\dot{\boldsymbol{q}} \end{pmatrix} \tag{48}$$

where

- $\bar{\mathbf{M}}$ is the generalized mass matrix

$\mathbf{C}_q$ is the Jacobian matrix of constraints
$\mathbf{0}$ is a zero matrix
$\boldsymbol{\lambda}$ is the vector of Lagrange multipliers for each constraint
$\ddot{\boldsymbol{q}}$ is the second time derivative of the generalized coordinate vector $\boldsymbol{q}$.
$\boldsymbol{f}$ is the vector with generalized forces
$\mathbf{C}_{qq}$ is the Jacobian matrix of $\mathbf{C}_\mathbf{q}\dot{\boldsymbol{q}}$ over $\boldsymbol{q}$, which includes the terms that do not depend on the accelerations.

From this description it is possible to determine the second derivative of the generalized coordinates $\ddot{\boldsymbol{q}}$. Since all other variables only depend on $\boldsymbol{q}$ and $\dot{\boldsymbol{q}}$, it is possible to integrate the system over time. The vector of Lagrange multipliers $\boldsymbol{\lambda}$ can be used to find the forces applied by the caregiver and the castor wheel.

D. Integration of equations of motion over time

Once the equations of motion have been derived, an integration scheme can be used to find a solution over time. If Assumption 12 is used, there are no degrees of freedom in velocity space. The state of the system $\boldsymbol{Y}$ is defined as

$$\boldsymbol{Y} = \begin{pmatrix} \boldsymbol{q} \\ \dot{\boldsymbol{q}} \end{pmatrix} \tag{49}$$

and its derivative

$$\dot{\boldsymbol{Y}} = \begin{pmatrix} \dot{\boldsymbol{q}} \\ \ddot{\boldsymbol{q}} \end{pmatrix} \tag{50}$$

During each integration step, $\ddot{\boldsymbol{q}}$ is determined by inverting Equation 48

$$\begin{pmatrix} \ddot{\boldsymbol{q}} \\ \boldsymbol{\lambda} \end{pmatrix} = \begin{pmatrix} \mathbf{M} & \mathbf{C}_q^{\mathrm{T}} \\ \mathbf{C}_q & \mathbf{0} \end{pmatrix}^{-1} \begin{pmatrix} \boldsymbol{f} \\ \mathbf{C}_{qq}\dot{\boldsymbol{q}} \end{pmatrix} \tag{51}$$

To execute this integration, the MATLAB function `ode45` was used. Due to the kinematic constraints given in Equations 39 to 44, not all states are feasible. To guarantee that the initial condition is feasible the Gauss-Newton method is used to project the initial condition on the constraint space. This coordinate projection can also be used during the simulation to correct deviations from the constraint space if the deviation from the constraints is too large. An estimate of the state is chosen as

$$\bar{\boldsymbol{Y}} = \begin{pmatrix} \bar{\boldsymbol{q}} \\ \bar{\dot{\boldsymbol{q}}} \end{pmatrix}, \tag{52}$$

and the error on the state is defined in configuration space as

$$\boldsymbol{Y} = \bar{\boldsymbol{Y}} + \Delta\boldsymbol{Y}, \tag{53}$$

where

$\boldsymbol{Y}$ is the true state where the kinematic constraints are satisfied,
$\bar{\boldsymbol{Y}}$ is the estimate of the state,
$\Delta\boldsymbol{Y}$ is the error between the true and estimate state.

In appendix F the implementation of the constraint projection is shown.

E. Determining the reaction forces from the Lagrange multipliers

The main forces of interest are F_t on the castor, M'_P on the wheelchair in the down direction by the caregiver, and F_P on the push handle by the caregiver. Each of these reactions is governed by a constraint, $C_{\mathrm{C\_tangent}}$, $C_{\mathrm{B\_fixed\_rotation}}$, and $C_{\mathrm{B\_fixed\_velocity}}$ respectively. We can use the corresponding Lagrange multipliers $\lambda_{\mathrm{C\_tangent}}$, $\lambda_{\mathrm{B\_fixed\_rotation}}$, and $\lambda_{\mathrm{B\_fixed\_velocity}}$ to find

$$F_t = -\lambda_{\mathrm{C\_tangent}}, \tag{54}$$
$$F_P = -\lambda_{\mathrm{B\_fixed\_velocity}}, \tag{55}$$
$$M'_P = -\lambda_{\mathrm{B\_fixed\_rotation}}. \tag{56}$$

V. Simulation protocol

In the simulation protocol, the methods to generate the results are shown.

A. Variables and parameters

By default, the variables from Table II are used unless specified otherwise. During each simulation the system is simulated until steady-state is reached. Steady-state is quantified as movement where the time derivative of the swivel angle $\dot{\delta}$ has converged to a value smaller than $0.01\,\mathrm{rad/s}$. Usually this is achieved within one second of simulation. Table III shows the simulations that are performed using this method. Each simulation is executed for both $\phi_x = 0\,\mathrm{rad}$ and $\phi_x = 0.1\,\mathrm{rad}$.

B. Protocol of comparison between steady-state approximation and multibody dynamics model

The results from the multibody dynamics model and the steady-state approximation are compared by plotting both solutions. The lateral force on the castor F_t, the sum of moments not applied by the caregiver $M'_{\neg P}$, and the push force by the caregiver F_P.

C. Protocol of the lateral force on the castor wheel

The lateral force on the castor wheel F_t is calculated using Equation 25 as a function of the inverse of the turn radius r_{turn}^{-1}. The swivel angle δ is taken from the multibody simulation which has converged to steady-state. To plot Equation 25 as a function of r_{turn}^{-1} explicitly, the turn radius can also be calculated as a function of δ using the analytic derivation of the turn radius given in Equation A.75.

D. Protocol of influence of design parameters on the force and moment applied by the caregiver.

The push force of the user F_P and the moment on the system excluding the caregiver $M'_{\neg P}$ can be calculated using Equation 15 and 21 in steady-state. Both of these equations have three summed terms that contribute to the final value. The term $a_{\mathrm{f1}}F_{\mathrm{B1,D}}$ does not contribute because $a_{\mathrm{f1}} = 0$ in the considered case. Simulation 2 and 3 with wheel bank angle σ

Generalized coordinates	Unit	Initial value
x_B	m	0
y_B	m	0
ζ_z	rad	0
θ	rad	0
δ	rad	0
z_D	m	$-r_w - L_{\mathrm{df}}$
$\dot{x}_B$	m/s	0 *
$\dot{y}_B$	m/s	0 *
$\dot{\zeta}_z$	rad/s	0 *
$\dot{\theta}$	rad/s	0 *
$\dot{\delta}$	rad/s	0 *
$\dot{z}_D$	m/s	0 *
Design parameters	Unit	Default value
r_w	m	0.095
r_r	m	0.28
L_{ex}	m	0.05
L_{ey}	m	0
L_{df}	m	0.175
a_P	m	-0.1
σ	rad	0
ϕ_x	rad	0 and 0.1
ϕ_y	rad	0
a_{f1}	m	0.44
b_{ri}	m	0
b_{f1}	m	0
b_{r1}	m	0.56/2
b_{r2}	m	$-b_{\mathrm{r1}}$
m_w	kg	0 (negligible)
m_f	kg	0 (negligible)
m_{wc}	kg	1000/9.81
Environment parameters	Unit	Default value
$f_{\mathrm{r,fi}}$	–	0.02
$f_{\mathrm{r,ri}}$	–	0.005
g	m/s^2	9.81
Use variables	Unit	Default value
v_{wc}	m/s	0.8
r_{turn}	m	1000
M_P	Nm	0 *
F_P	N	0 *
P_f	–	1/3
b_P	m	0.283

TABLE II: Default parameter values (* driven by constraint)

proved to have very little influence, so these simulations are omitted.

The push location b_P can be found by calculating $M'_{\neg P}/F_P$ (Equation 22). The push location is found for both a hard smooth surface, and on a carpet.

VI. Results

In the results section the figures corresponding to the sections of the protocol in section V are shown, and a short description is given.

A. Graphs of comparison between steady-state approximation and multibody dynamics model

The Lagrange and TMT method yield numerically equivalent results, so either can be used. The comparison between the TMT method and steady-state approximation is plotted in Figure 7 for simulation 1. Figures 7a, 7b, and 7c show the lateral force F_t on the castor wheel, the moment $M'_{\neg P}$, and the required pushing force F_P respectively. Note that the moment $M'_{\neg P}$ is the antagonist of M'_P, so $M'_P = -M'_{\neg P}$, as was shown in Equation 19.

The lines correspond to the solutions found with the TMT method. The dot '$\cdot$' markers are derived using the moment around the swivel axis (Equation 23) in steady-state without the small-angle approximation. The cross '$\times$' markers correspond to the simplified Equations 15, 21, and 25. A selection of results is presented here. The rest can be found on the TU Delft repository.[3]

B. Graphs of the lateral force on the castor wheel

Out of the parameters varied in simulations 1 to 6, only ϕ_x alters the lateral force on the castor wheel when the wheelchair is driving in a straight line. Therefore the results for the other simulations are calculated for $\phi_x = 0.1\,\mathrm{rad}$. The lateral force F_t is shown in Figure 8 for simulations 1 to 6. The cases where the wheelchair drives on a carpet and on a hard, smooth surface are both plotted. Only in Figure 8b the roll resistance has an effect on F_t.

C. Graphs of influence of design parameters on the force and moment applied by the user.

In Figures 9 to 12, the top left subfigure is the lateral force on the castor F_P, and the top right subfigure is the moment $M'_{\neg P}$. The variation of F_P to the roll resistance is shown in the bottom left subfigures. The moment $M'_{\neg P}$ only has minimal dependence on the roll resistance, so this result is omitted.

The push location $b_P = M'_{\neg P}/F_P$ is shown in the bottom right subfigure in Figures 9 to 12. The red line corresponds to the minimum size of b_P, which is the distance between the symmetry plane and the right rear wheel b_{r1}. Because the push force F_P can cross zero, the push location b_P often has asymptotes which correspond to the zero crossings of F_P.

VII. Discussion

In the discussion, the results are interpreted, and recommendations for future research are given.

A. Accuracy of the steady-state approximation

Both the steady-state approximation (visualized with '$\cdot$') and its small-angle approximation (visualized with '$\times$') correlate closely with the multibody model. The largest absolute difference in experiment 1 (Figure 7) between the small-angle approximation and MBD model on $M'_{\neg P}$ is $0.74\,\mathrm{N}$. On the push force F_P the largest absolute error is $0.89\,\mathrm{N}$. This corresponds to $8\,\%$ and $1.8\,\%$ respectively.

The reason that the absolute error on the moment can be large is that the multibody model has a roughly constant offset from the steady-state approximation. If the moment calculated by the multibody model approaches zero, the denominator to calculate the percentage difference converges to zero.

[3] https://repository.tudelft.nl/

simulation number	Variable 1 (x-axis)				Variable 2 (lines)			
	Variable	Unit	Value min	Value max	Variable	Unit	Value min	Value max
1	$1/r_{\text{turn}}$	m^{-1}	-1	1	ϕ_x	rad	-0.2	0.2
2	$1/r_{\text{turn}}$	m^{-1}	-1	1	σ	rad	-0.2	0.2
3	$1/r_{\text{turn}}$	m^{-1}	-1	1	$\sigma*$	rad	-0.2	0.2
4	$1/r_{\text{turn}}$	m^{-1}	-1	1	ϕ_y	rad	-0.2	0.2
5	$1/r_{\text{turn}}$	m^{-1}	-1	1	v_{wc}	m/s	-0.8	0.8
6	$1/r_{\text{turn}}$	m^{-1}	-1	1	P_f	–	0	1
7	P_f	–	0	0.1	ϕ_x	rad	-0.2	0.2

TABLE III: Overview of performed simulations (* in simulation 3 L_{df} and L_{ex} are chosen such that Equations 37 and 38 hold). Variable 1 is used as the x-axis of the plots, and a line is drawn for multiple values of Variable 2.

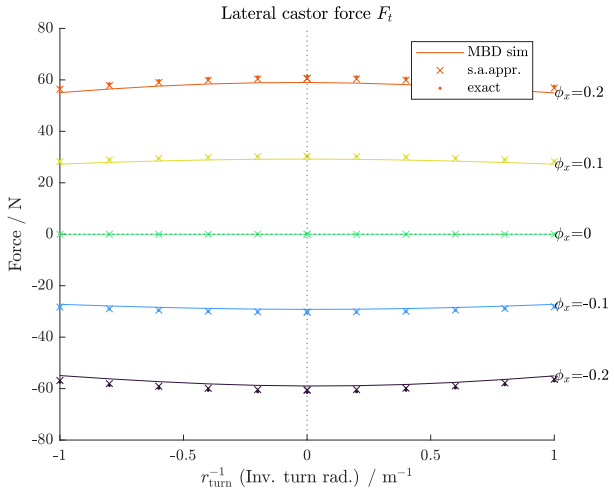

(a) Sim. 1: Lateral force on castor wheel given turn radius r_{turn} and cant angle ϕ_x.

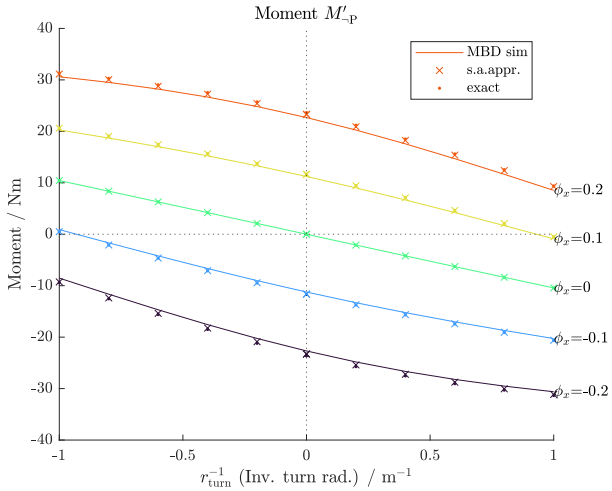

(b) Sim. 1: Moment $M'_{\neg P}$ exerted on wheelchair in down direction given turn radius r_{turn} and cant angle ϕ_x.

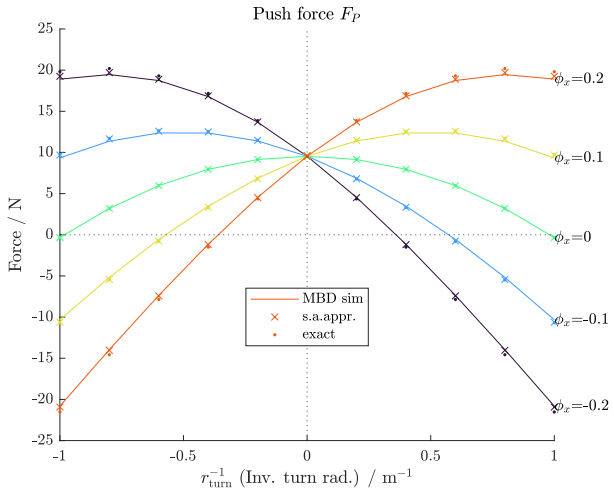

(c) Sim. 1: Force F_P exerted in forward direction on B by caregiver given turn radius r_{turn} and cant angle ϕ_x.

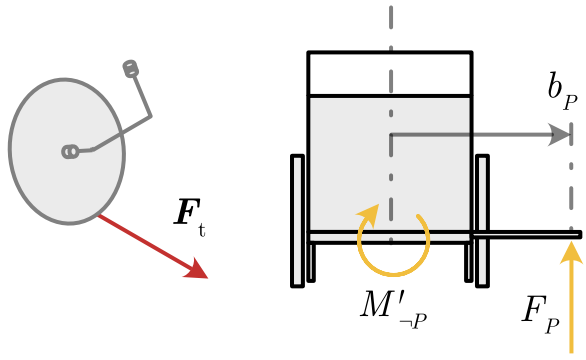

(d) Quick reference of variables used in the plots, simplified from Figure 3 and Figure 6d. $M'_{\neg P}$ is defined in Equation 19.

Fig. 7: Exp 1: Comparison between the multibody model (MBD sim), the steady-state approximation (exact), and the small-angle approximation of steady-state approximation (s. a. approx.). A more positive r_{turn}^{-1} is a sharp turn to the right, and a more negative r_{turn}^{-1} is a sharper turn to the left.

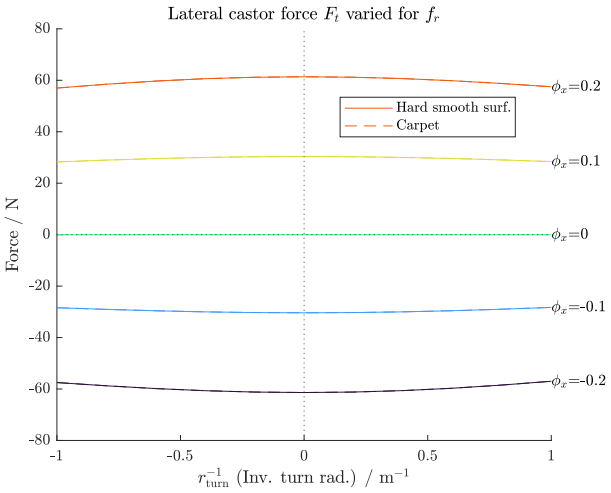

(a) Sim. 1: Lateral force F_t for ϕ_x as function of r_{turn}.

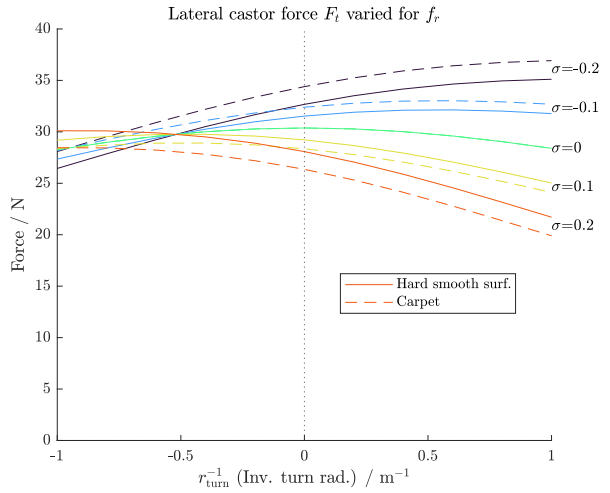

(b) Sim. 2: Lateral force F_t for σ as function of r_{turn} in a case where $\phi_x = 0.1\,\text{rad}$.

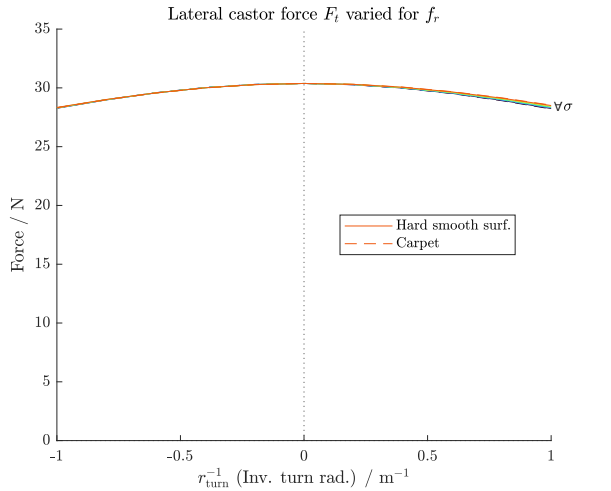

(c) Sim. 3: Lateral force F_t for σ as function of r_{turn} in a case where $\phi_x = 0.1\,\text{rad}$, and where the design parameters are chosen such that point C does not move laterally when wheel bank angle σ is changed.

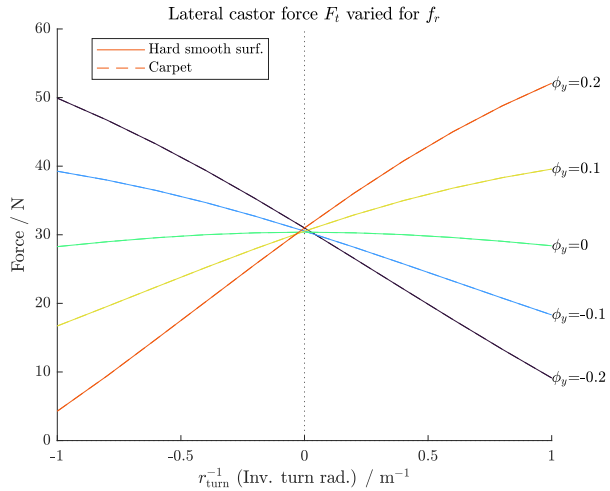

(d) Sim. 4: Lateral force F_t for ϕ_y as function of r_{turn} in a case where $\phi_x = 0.1\,\text{rad}$.

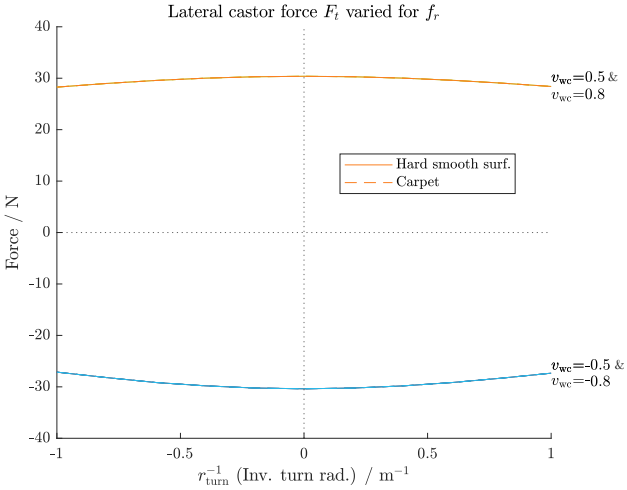

(e) Sim. 5: Lateral force F_t for v_{wc} as function of r_{turn} in a case where $\phi_x = 0.1\,\text{rad}$.

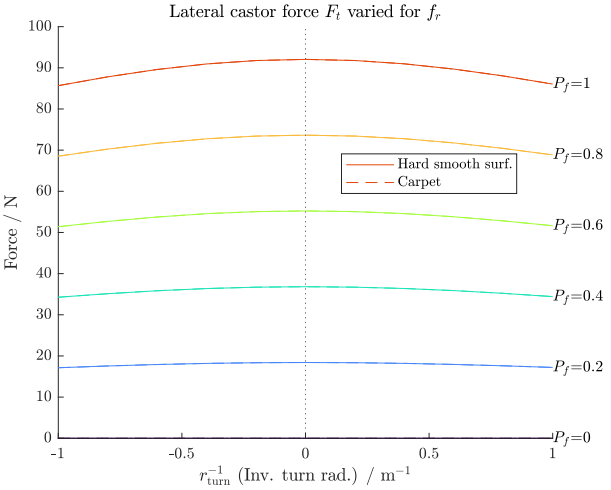

(f) Sim. 6: Lateral force F_t for P_f as function of r_{turn} in a case where $\phi_x = 0.1\,\text{rad}$. Note that the forward location of the center of mass $a_G = a_{\text{f1}} P_f$ (Equation 8).

Fig. 8: The lateral force F_t on the castor wheel as a function of the turn radius r_{turn} for simulations 1 to 6. For all simulations except 2 the rolling resistance has no effect on F_t.

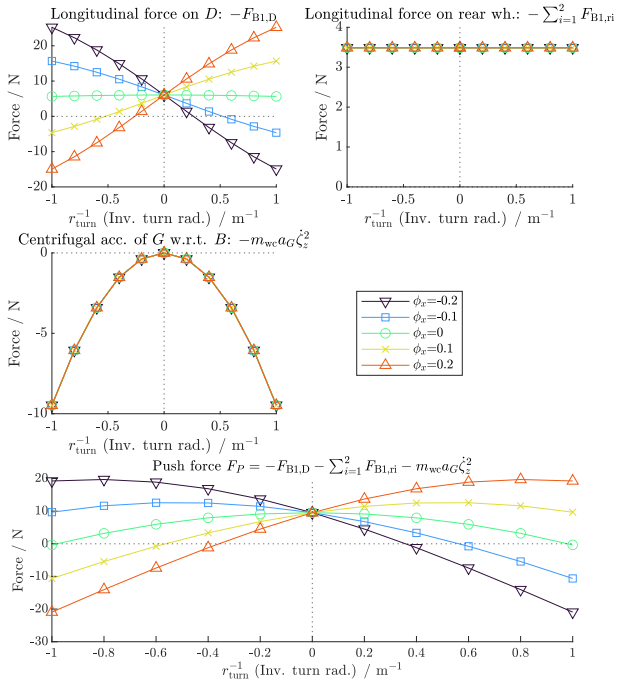

(a) Sim. 1: Push force F_P split in the terms of Equation 15 as a function of the inverse turn radius r_{turn}^{-1} for different cant angles ϕ_x. The bottom plot of F_P is equal to the sum of the plots above.

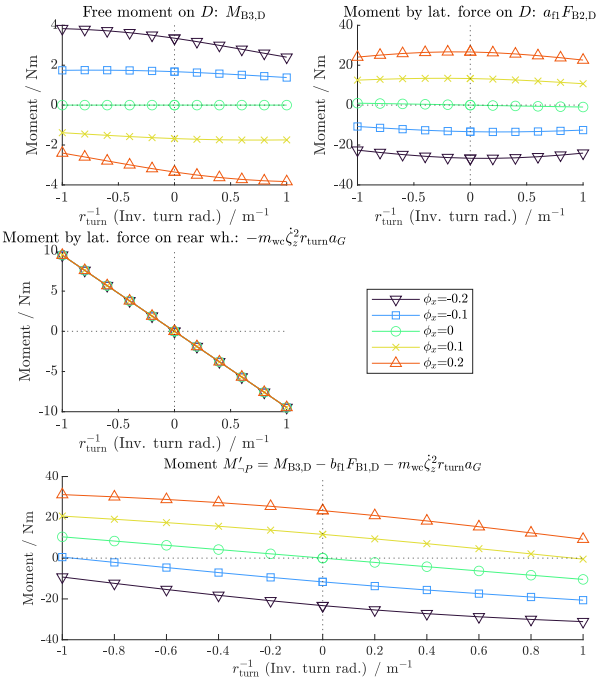

(b) Sim. 1: Moment $M'_{\neg P}$ split in the terms of Equation 21 as a function of the inverse turn radius r_{turn}^{-1} for different cant angles ϕ_x. The term $a_{\mathrm{fl}} F_{\mathrm{B1,D}}$ does not contribute because $a_{\mathrm{fl}} = 0$ in the considered case. The rolling resistance has almost no effect on the components of $M'_{\neg P}$. The bottom plot of $M'_{\neg P}$ is equal to the sum of the plots above.

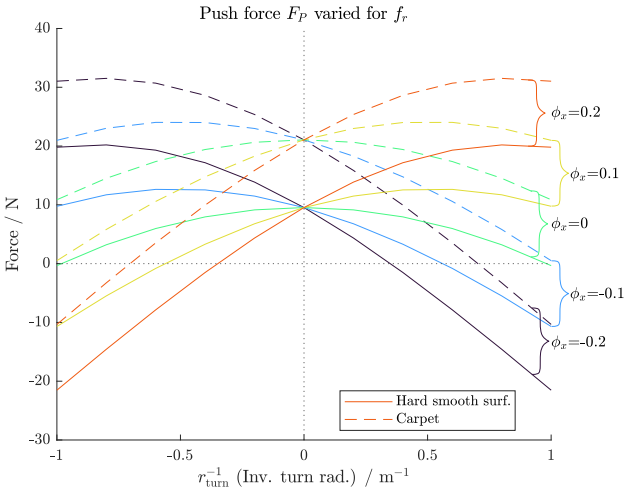

(c) Sim. 1: Force F_P in forward direction on point P by caregiver given turn radius r_{turn} for different cant angles ϕ_x, varied for roll resistances. The values for the roll resistance are given in Table I.

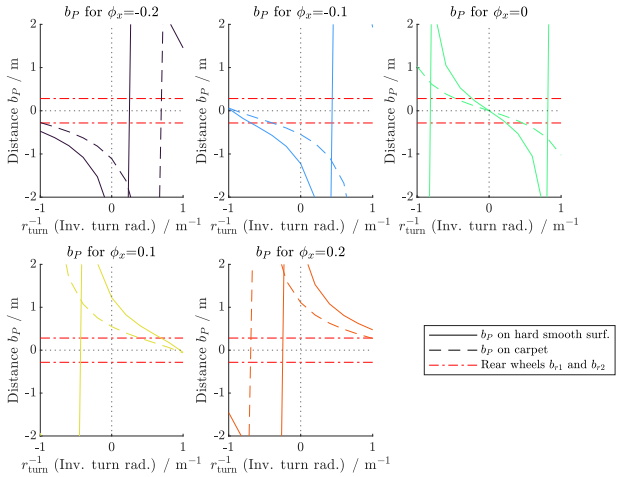

(d) Sim. 1: Push location b_P as a function of the inverse turn radius r_{turn}^{-1} for different cant angles ϕ_x. The push location b_P is calculated for a case where the caregiver does not apply a free moment M_P, using $b_P = M'_{\neg P}/F_P$ (Equation 22).

Fig. 9: Sim. 1: Overview of the effects of the **cant angle** ϕ_x on the push force F_P, moment $M'_{\neg P}$, and push location b_P of the wheelchair as a function of the inverse turn radius r_{turn}^{-1}. A more positive r_{turn}^{-1} is a sharp turn to the right, and a more negative r_{turn}^{-1} is a sharper turn to the left.

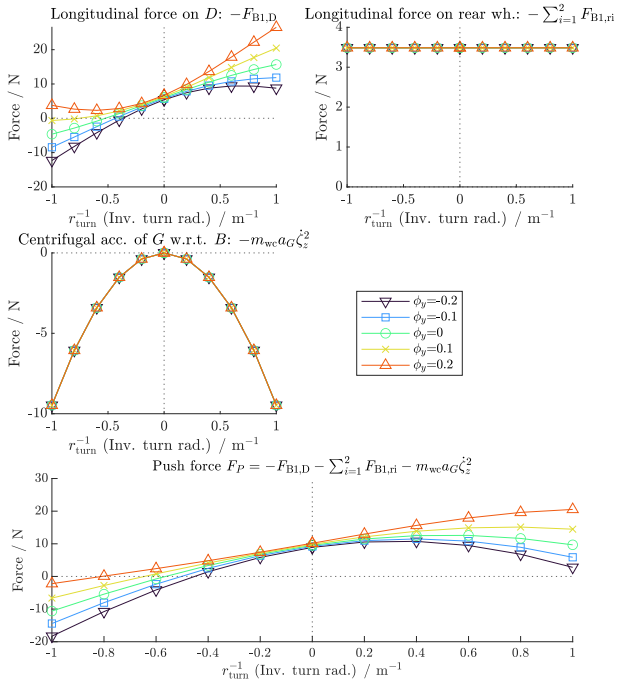

(a) Sim. 4: Push force F_P split in the terms of Equation 15 as a function of the inverse turn radius r_{turn}^{-1} for different rake angles ϕ_y given $\phi_x = 0.1\,\mathrm{rad}$. The bottom plot of F_P is equal to the sum of the plots above.

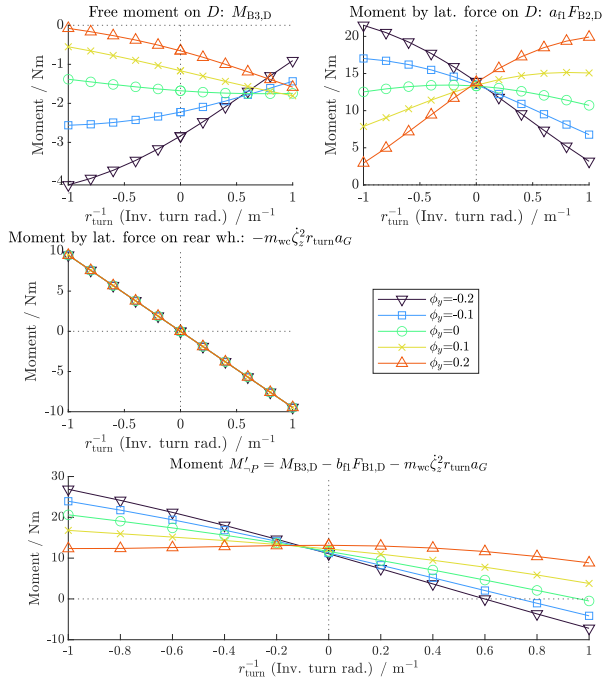

(b) Sim. 4: Moment $M'_{\neg P}$ split in the terms of Equation 21 as a function of the inverse turn radius r_{turn}^{-1} for different rake angles ϕ_y given $\phi_x = 0.1\,\mathrm{rad}$. The term $a_{\mathrm{fl}} F_{\mathrm{B1,D}}$ does not contribute because $a_{\mathrm{fl}} = 0$ in the considered case. The rolling resistance has almost no effect on the components of $M'_{\neg P}$. The bottom plot of $M'_{\neg P}$ is equal to the sum of the plots above.

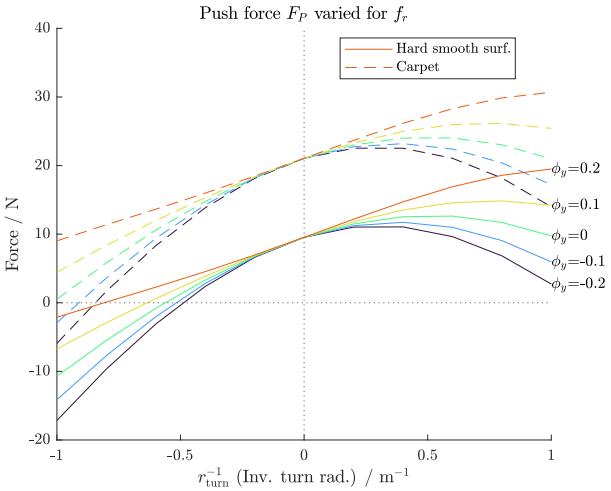

(c) Sim. 4: Force F_P in forward direction on point P by caregiver as a function of the inverse turn radius r_{turn}^{-1} for different rake angles ϕ_y given $\phi_x = 0.1\,\mathrm{rad}$, varied for roll resistances. The values for the roll resistance are given in Table I.

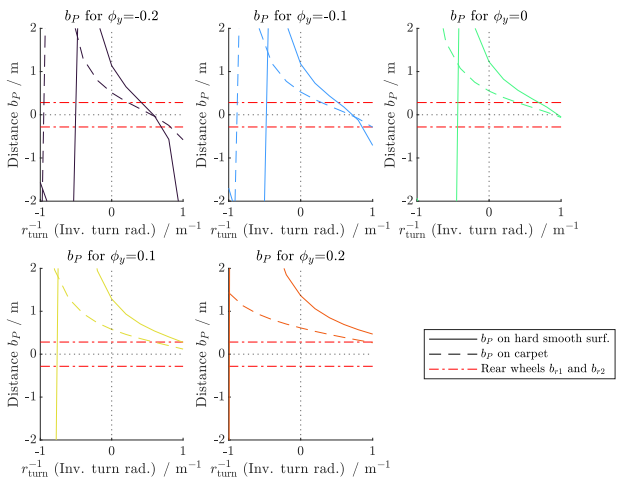

(d) Sim. 4: Push location b_P as a function of the inverse turn radius r_{turn}^{-1} for different rake angles ϕ_y given $\phi_x = 0.1\,\mathrm{rad}$. The push location b_P is calculated for a case where the caregiver does not apply a free moment M_P, using $b_P = M'_{\neg P}/F_P$ (Equation 22).

Fig. 10: Sim. 4: Overview of the effects of the **rake angle** ϕ_y on the push force F_P, moment $M'_{\neg P}$, and push location b_P of the wheelchair as a function of the inverse turn radius r_{turn}^{-1} for a case where cant angle $\phi_x = 0.1\,\mathrm{rad}$. A more positive r_{turn}^{-1} is a sharp turn to the right, and a more negative r_{turn}^{-1} is a sharper turn to the left.

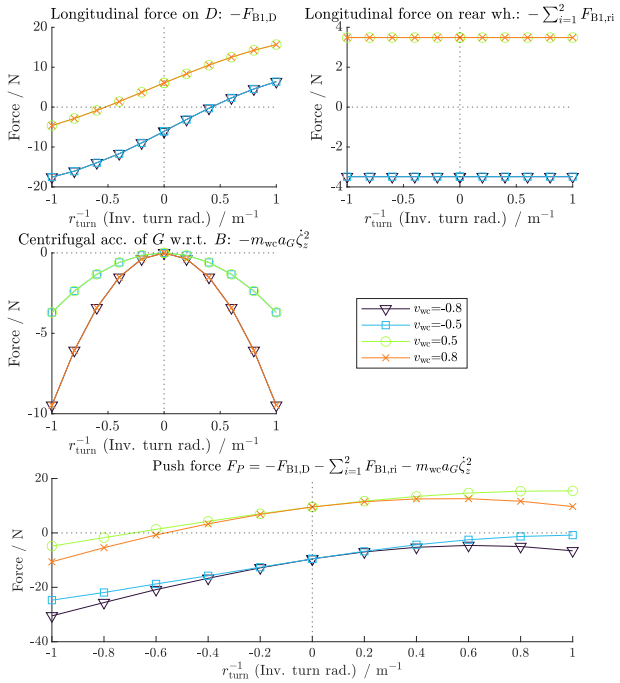

(a) Sim. 5: Push force F_P split in the terms of Equation 15 as a function of the inverse turn radius r_{turn}^{-1} for different forward velocities v_{wc} given $\phi_x = 0.1\,\mathrm{rad}$. The bottom plot of F_P is equal to the sum of the plots above.

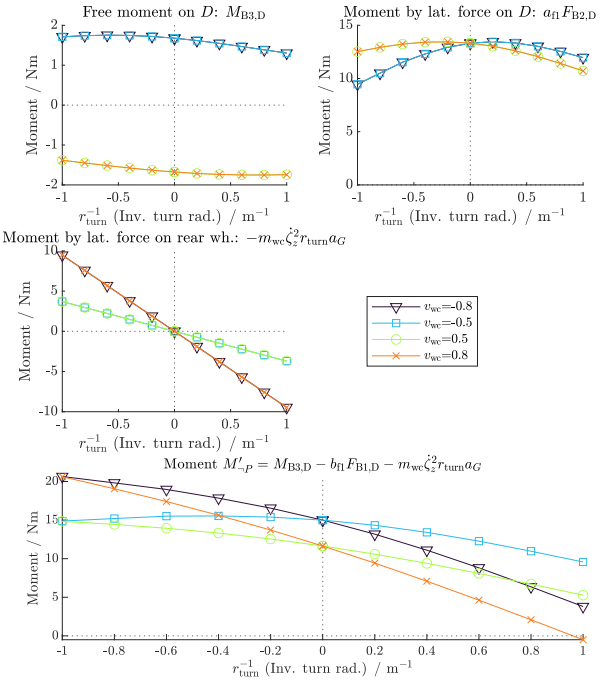

(b) Sim. 5: Moment $M'_{\neg P}$ split in the terms of Equation 21 as a function of the inverse turn radius r_{turn}^{-1} for different forward velocities v_{wc} given $\phi_x = 0.1\,\mathrm{rad}$. The term $a_{\mathrm{fl}} F_{\mathrm{B1,D}}$ does not contribute because $a_{\mathrm{fl}} = 0$ in the considered case. The rolling resistance has almost no effect on the components of $M'_{\neg P}$. The bottom plot of $M'_{\neg P}$ is equal to the sum of the plots above.

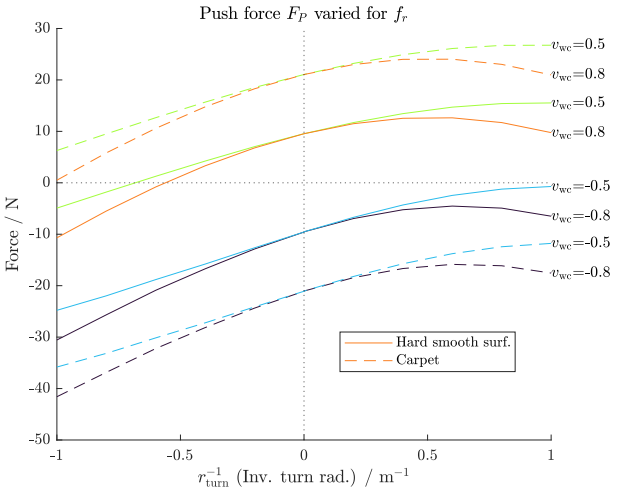

(c) Sim. 5: Force F_P in forward direction on point P by caregiver as a function of the inverse turn radius r_{turn}^{-1} for different forward velocities v_{wc} given $\phi_x = 0.1\,\mathrm{rad}$, varied for roll resistances. The values for the roll resistance are given in Table I.

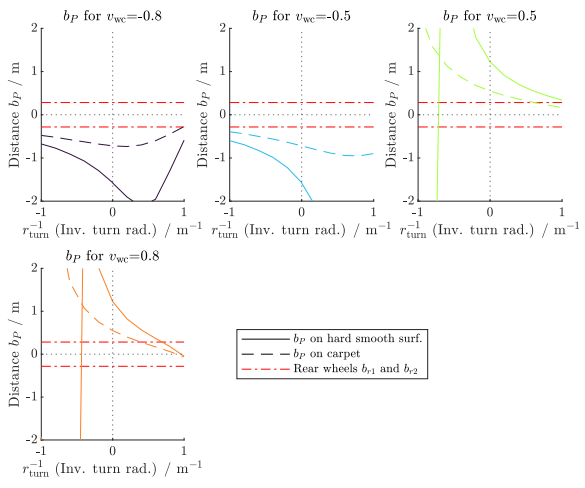

(d) Sim. 5: Push location b_P as a function of the inverse turn radius r_{turn}^{-1} for different forward velocities v_{wc} given $\phi_x = 0.1\,\mathrm{rad}$. The push location b_P is calculated for a case where the caregiver does not apply a free moment M_P, using $b_P = M'_{\neg P}/F_P$ (Equation 22).

Fig. 11: Sim. 5: Overview of the effects of the **forward velocity** v_{wc} on the push force F_P, moment $M'_{\neg P}$, and push location b_P of the wheelchair as a function of the inverse turn radius r_{turn}^{-1} for a case where cant angle $\phi_x = 0.1\,\mathrm{rad}$. A more positive r_{turn}^{-1} is a sharp turn to the right, and a more negative r_{turn}^{-1} is a sharper turn to the left.

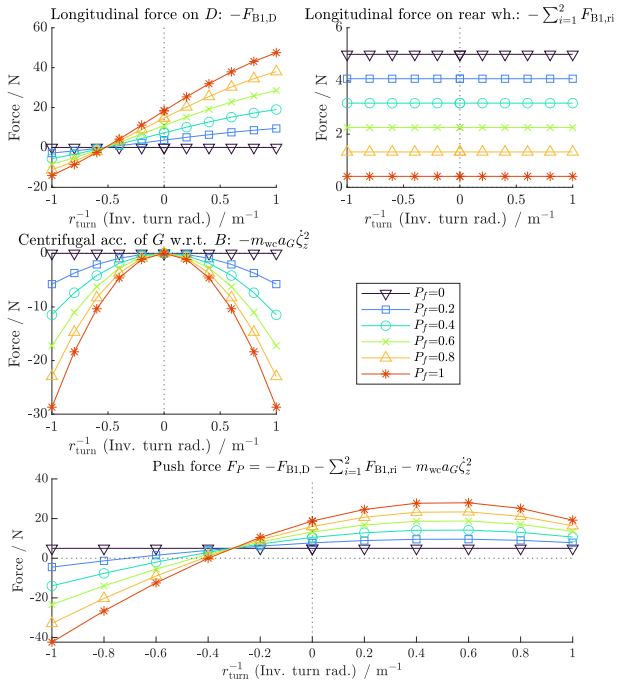

(a) Sim. 6: Push force F_P split in the terms of Equation 15 as a function of the inverse turn radius r_{turn}^{-1} for different fractions of weight on the front wheels P_f given $\phi_x = 0.1\,\mathrm{rad}$. The bottom plot of F_P is equal to the sum of the plots above.

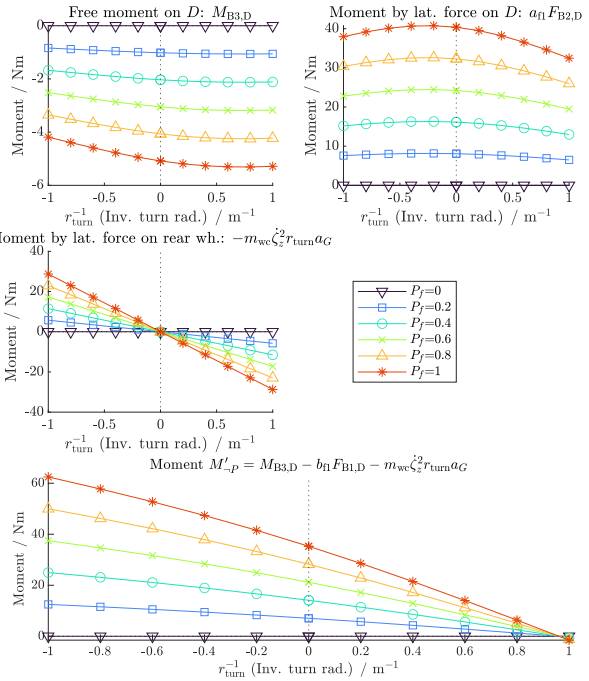

(b) Sim. 6: Moment $M'_{\neg P}$ split in the terms of Equation 21 as a function of the inverse turn radius r_{turn}^{-1} for different fractions of weight on the front wheels P_f given $\phi_x = 0.1\,\mathrm{rad}$. The term $a_{\mathrm{fl}} F_{\mathrm{B1,D}}$ does not contribute because $a_{\mathrm{fl}} = 0$ in the considered case. The rolling resistance has almost no effect on the components of $M'_{\neg P}$. The bottom plot of $M'_{\neg P}$ is equal to the sum of the plots above.

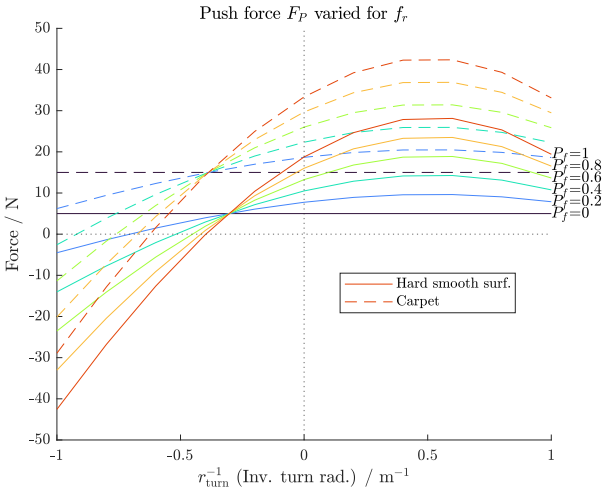

(c) Sim. 6: Force F_P in forward direction on point P by caregiver as a function of the inverse turn radius r_{turn}^{-1} for different fractions of weight on the front wheels P_f given $\phi_x = 0.1\,\mathrm{rad}$, varied for roll resistances. The values for the roll resistance are given in Table I.

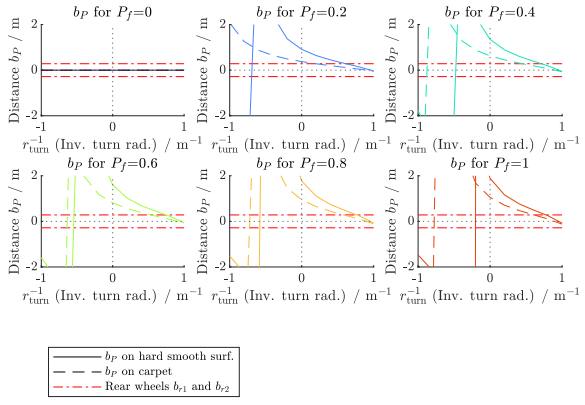

(d) Sim. 6: Push location b_P as a function of the inverse turn radius r_{turn}^{-1} for different fractions of weight on the front wheels P_f given $\phi_x = 0.1\,\mathrm{rad}$. The push location b_P is calculated for a case where the caregiver does not apply a free moment M_P, using $b_P = M'_{\neg P}/F_P$ (Equation 22).

Fig. 12: Sim. 6: Overview of the effects of the **fraction of weight on the front wheels** P_f on the push force F_P, moment $M'_{\neg P}$, and push location b_P of the wheelchair as a function of the inverse turn radius r_{turn}^{-1} for a case where cant angle $\phi_x = 0.1\,\mathrm{rad}$. A more positive r_{turn}^{-1} is a sharp turn to the right, and a more negative r_{turn}^{-1} is a sharper turn to the left.

B. Influence of parameters

The lateral castor force F_t is roughly linearly dependent on the cant angle, as was determined in Equation 25. This makes the cant angle an good choice to increase moment $M'_{\neg P}$ and move the push location b_P to the positive right side, as was also found by Bennett [10].

The pushing force F_P is not affected by the cant angle ϕ_x, rake angle ϕ_x, or wheel bank angle σ when the wheelchair moves in a straight line (Figure 9c, $r_{\text{turn}}^{-1} = 0$). The direction of the rolling resistance on the castor wheel $\hat{\boldsymbol{l}}$ must point in the direction of movement due to the no-slip assumption. The magnitude of the rolling resistance is assumed to be only a function of the vertical load and the rolling resistance coefficient. Since the magnitude and direction of $\boldsymbol{F}_l$ are equal, the pushing force F_P is unaffected.

Rolling resistance on the front wheel can have effects on the lateral force F_t on the castor wheel as was shown in Figure 8b. This is not a desirable characteristic, as rolling resistance depends on the surface type of the environment. To prevent this, the moment arm between the swivel axis $\hat{\boldsymbol{d}}_3$ and longitudinal force $\boldsymbol{F}_l$ should be as small as possible. In experiment 1, L_{ey} and σ are zero (see kinematic diagram in Figure 6b). This means that F_t is independent from the rolling resistance factor $f_{\text{r,fi}}$.

The roll resistance and the lateral force on the castor scale linearly with the total weight of the wheelchair and occupant m_{wc}. Therefore, the total weight does not affect the push location b_P. The longitudinal location of the center of mass a_G does have an effect, as is shown in Figure 12d. The weight distribution between the front and rear wheels depends on the body weight of the occupant and the design of the wheelchair.

The magnitude of the forward velocity v_{wc} has no effect on the lateral force F_t on the castor (Figure 8e), but does influence the terms in F_P and $M'_{\neg P}$ that depend on $\dot{\zeta}_z$ considerably, due to the centripetal acceleration in Equation 15. Even for a conventional wheelchair, a forward velocity of $0.8\,\text{m}$ is sufficient to reduce the push force to zero on a hard smooth surface (Figure 9a, $\phi_x = 0$) when the wheelchair drives in a sharp turn with a turn radius r_{turn} of $1\,\text{m}$. These centripetal terms were ignored in some studies [20]–[22], where it is assumed that the acceleration of the center of mass is only straight forward due to $\dot{v}_{\text{wc}}$.

C. Recommendations for design parameters

Good design parameters for a wheelchair pushed from the side should allow the user to push on the push bar without applying a free moment M_P. For usability, the lateral location of point P must be right next to the wheelchair or further out.

The roll resistance has a large effect on push location b_P. This variability is so large because the moment $M'_{\neg P}$ changes very little with roll resistance, while the required pushing force shown in Figure 9a is linearly dependent on it for a straight trajectory (Equation 16). The minimum length for a bar that could push the wheelchair in a straight line on both surface types is $b_P = 0.61\,\text{m}$ for $\phi_x = 0.5\,\text{rad}$, measured from the symmetry plane of the wheelchair. This value can be determined by tuning parameters in Figure 9d such that the lines for b_P for both surface types are above b_{r1}. An additional free moment M_P would still be required to make sharp turns in either direction if b_P is below the red line in Figure 9d, or exceeds length of the push bar.

When F_P converges to zero, b_P diverges to infinity. The pushing force can become zero due to the inertial term in Equation 15. This inertial term always decreases F_P because $-a_G\dot{\zeta}_z^2$ is always negative. To a smaller extent, the lateral force F_t on the castor can also reduce F_P as it can have a component in the backward direction, which is shown in Equation 30. To make tighter turns, the caregiver must apply a moment M_P in addition to the pushing force. The magnitude of this moment can be calculated using $M'_P = M_P - b_p F_p$ (Equation 19).

The cant angle ϕ_x can be used to increase the lateral force on the castor F_t when the wheelchair moves in a straight line (Figure 8a). The rake angle modifies the slope of the lateral force with respect to the inverse turn radius (Figure 8d). By combining the cant and rake angle, slope and y-intersection of the lateral castor force F_t can be tuned.

The preferred position of the castor wheel is affected by the rake and cant angle. A positive rake angle causes the preferred position of the castor wheel to be in the backward direction (see Figure 5 B)). When the wheelchair is in the preferred position, the potential energy is minimal. To initiate movement of the wheelchair, the caregiver must overcome this energy deficiency before the wheelchair to push the wheelchair forward. The preferred position for a pure cant angle is to the side, which poses similar problems. The designer of a wheelchair must weigh the advantages of a desirable preferred position versus the steering characteristics provided by a positive rake angle, or design a different solution such that the preferred position is forward.

The weight distribution influences push location b_P as is shown in Figure 12d. To prevent this, a wheelchair could be designed such that the load on the castor wheel can be set arbitrarily.

D. Recommendations for future work

The small-angle approximation is sufficient to determine the reaction forces in steady-state. Therefore it is recommended to use this approach over the TMT and Lagrange approach when possible. If the moment and force of the caregiver are considered as a free input rather than a constraint (so not using uniform circular motion as was assumed in Assumption 12), then the steady-state approximation is no longer valid.

Real-world experiments should be performed to validate the model. A 6-axis force and torque sensor can be mounted between the wheelchair and the castor top plate. Most of these sensors are prone to damage caused by a bending moment. A test can be conducted with a reduced total weight to circumvent this. All forces and moments exerted by the ground on the wheelchair scale linearly with vertical load, so if an experiment is performed with half the weight, the reaction forces can be doubled to get the real values. Assumption 15 (castor wheel and fork have negligible weight) might be violated if the weight on the wheelchair is reduced too far.

The effect on the moment by the weight distribution shown in Figure 12b could be used to reduce the moment that the

caregiver has to apply. The vertical load on the castor could be controlled by attaching the castor wheel to the wheelchair with a flexible component, and support a part of the load via the regular castor wheels on the chair. If regular castor wheels support the wheelchair, then the force on the modified castor wheel is equal to the deflection of the flexible component times its stiffness. This solution could also allow the wheelchair to move in the backward direction easier by lowering the vertical load on the castor in this direction. A possible implementation could look similar to how the pitch of the wheelchair was considered in this study, shown in Figure 5.

In this work, it was assumed that the wheel is a flat disk. If the wheel has a width that is not negligible, the shape of the wheel can be approximated as a toroid. This approach was used by Garcia-Agundez et al. [13] to analyze the motion of a Waveboard.

During preparation for this study, it was considered whether the cant angle could also help wheelchair users navigate banked surfaces. Coolen et al. [26] investigate common skills required for wheelchair propulsion, including turns, banked surfaces, curbs, and wheelies. 100% of the study participants passed the side-slope test, meaning that few to no wheelchair users have trouble navigating side-sloped inclines.

This study focussed on the case where a caregiver pushes the occupant, but this model can also be applied to an occupant who propels the wheelchair by themself. In the introduction, it was discussed that people who have suffered a stroke also struggle with propelling the wheelchair in a straight line [2]. Introducing a small cant angle could help counteract the asymmetry of the propulsion.

VIII. Conclusion

This study established a relation between the pushing position of a caregiver and the design parameters of the castor wheel using a steady-state approximation and a multibody simulation. By choosing the parameters accordingly, a wheelchair can be designed to be pushed from a position next to the occupant.

The cant angle provides a lateral force without increasing the required pushing force for straight trajectories. The rake and wheel bank angles can modify the amplitude of this steering effect and can be used to tune the desired characteristics of the wheelchair. A positive rake angle reduces the slope of the steering moment for different turn radii and shifts the castor wheel's preferred position more in the backward direction. This situation allows the caregiver to achieve certain turn radii from a push position closer to the wheelchair, but is also more sensitive to the push force and location of the caregiver.

The weight distribution between the front and rear wheels influences the moment generated by the castor, but the magnitude of the total weight of the wheelchair and occupant does not.

The roll resistance affects the ideal location to push the wheelchair, because the push force is $F_P = 9.5\,\mathrm{N}$ at least and $21.01\,\mathrm{N}$ at most. This means that b_P can increase by a factor of 2.2 depending on the surface type.

It is unrealistic to push a three-wheeled wheelchair over any forward trajectory with arbitrary turn radii on both a carpet and a hard, smooth surface without ever applying a free moment on the push handle. When pushing a conventional wheelchair in a sharp curve from the rear it is also required to apply a free moment. It is recommended to design the wheelchair such that for straight trajectories, the push bar is long enough to push the wheelchair with a pure pushing force for both low and high rolling resistance. The caregiver can then apply an extra moment to make a turn.

For the considered parameters, a cant angle of $\phi_x = 0.05\,\mathrm{rad}$ allows the caregiver to achieve a straight trajectory for any surface type without applying a free moment. A rake angle of $\phi_y = 0.1\,\mathrm{rad}$ can be used to reduce the required free moment in sharper turns. This positive rake angle does shift the preferred position further in the reverse orientation. The push bar for this case must at least reach $b_P = 0.61\,\mathrm{m}$ to facilitate straight trajectories.

The model can be compared to real-world experimental results in future work. The approximation can then be used to choose suitable design parameters for wheelchairs and other wheeled vehicles with castor wheels. The modification can also be used for wheelchair users who propel their own wheelchair asymmetrically, such as people who have suffered a stroke.

Acknowledgements

The idea to use a cant angle to steer a wheelchair was conceived by Lucy Bennett, Heike Vallery, and Bram Sterke, who all worked together with Nicole van den Dries - Luitwieler from Rijndam Revalidation to help children with PIMD.

I thank Lucy Bennett for her practical mindset and near infinite enthusiasm, and my supervisor Heike Vallery for her guidance and keen eye for details. I want to express my gratitude to Bram Sterke, who helped me during the beginning of the project to set realistic goals and expectations.

I also express my gratitude to Nikki, Janessa, Heike, and Lucy, who all helped me shape an incoherent bunch of sentences into a proper thesis.

Lastly, I thank everyone who supported me personally, including my family, the "Project Group ++", the "Second Living Room", and my fluffy dog Einstein.

References

[1] K. Samuelsson and E. Wressle, "User satisfaction with mobility assistive devices: An important element in the rehabilitation process," *Disability and Rehabilitation*, vol. 30, pp. 551–558, 1 2008. [Online]. Available: http://www.tandfonline.com/doi/full/10.1080/09638280701355777

[2] K. H. Tsai, C. Y. Yeh, and H. C. Lo, "A novel design and clinical evaluation of a wheelchair for stroke patients," *International Journal of Industrial Ergonomics*, vol. 38, pp. 264–271, 3 2008. [Online]. Available: https://doi.org/10.1016/j.ergon.2007.09.007

[3] S. L. Soltau, J. S. Slowik, P. S. Requejo, S. J. Mulroy, and R. R. Neptune, "An investigation of bilateral symmetry during manual wheelchair propulsion," *Frontiers in Bioengineering and Biotechnology*, vol. 3, 2015. [Online]. Available: /pmc/articles/PMC4464056/?report=abstracthttps://www.ncbi.nlm.nih.gov/pmc/articles/PMC4464056/

[4] M. A. Gallagher, F. Cuomo, L. Polonsky, K. Berliner, and J. D. Zuckerman, "Effects of age, testing speed, and arm dominance on isokinetic strength of the elbow," *Journal of Shoulder and Elbow Surgery*, vol. 6, pp. 340–346, 1997. [Online]. Available: https://pubmed.ncbi.nlm.nih.gov/9285873/

[5] V. S. Munde, C. Vlaskamp, W. Ruijssenaars, B. Maes, and H. Nakken, *Alertness and Learning of Individuals with PIMD*. Boston, MA: Springer US, 2012, pp. 195–197. [Online]. Available: https://doi.org/10.1007/978-1-4419-1428-6_718
[6] T. Kalinksy. (2013) Side-by-side push handle for wheelchair. [Online]. Available: https://www.tammykdesign.com/portfolio
[7] K. J. Davis, "Wheelchair wonderbar patent," U.S. Patent US20090302570A1, 2008. [Online]. Available: https://patents.google.com/patent/US20090302570
[8] B. R. Umberger, K. G. M. Gerritsen, and P. E. Martin, "A model of human muscle energy expenditure," *Comput. Methods Biomech. Biomed. Engin.*, vol. 6, no. 2, pp. 99–111, Apr. 2003. [Online]. Available: https://doi-org.tudelft.idm.oclc.org/10.1080/1025584031000091678
[9] L. Storch, "Manual wheelchair doesn't veer off toward curb on sidewalks," U.S. Patent US9080660B2, 2012. [Online]. Available: https://patents.google.com/patent/US9080660
[10] L. Bennett, "Design and development of a passive wheelchair mechanism to enable direction control," Delft University of Technology, Tech. Rep., 7 2020. [Online]. Available: https://conf.bme2021.nl/program/show_slot/11
[11] "ISO 7176-22:2017(en) wheelchairs - part 26: Vocabulary," Geneva, CH, 2007. [Online]. Available: https://www.iso.org/obp/ui/#iso:std:iso:7176:-26:ed-1:v1:en
[12] I. Besselink, "Shimmy of aircraft main landing gears," Ph.D. dissertation, Delft University of Technology, 2000. [Online]. Available: https://research.tue.nl/en/publications/shimmy-of-aircraft-main-landing-gears
[13] A. Garcia-Agundez, D. Garcia-Vallejo, and E. Freire, "Study of the forward locomotion of a three-dimensional multibody model of a waveboard by inverse dynamics," *Mechanism and Machine Theory*, vol. 149, 2020. [Online]. Available: https://www.scopus.com/inward/record.uri?eid=2-s2.0-85079538490&doi=10.1016%2fj.mechmachtheory.2020.103826&partnerID=40&md5=e55ab27e77c6d6a8e99b82b3d3204ba3
[14] R. Rajagopalan, "A generic kinematic formulation for wheeled mobile robots," *Journal of Robotic Systems*, vol. 14, pp. 77–91, 2 1997. [Online]. Available: https://onlinelibrary.wiley.com/doi/10.1002/(SICI)1097-4563(199702)14:2⟨77::AID-ROB3⟩3.0.CO;2-Q
[15] D. de Falco, G. Di Massa, and S. Pagano, "On the castor dynamic behavior," *Journal of the Franklin Institute*, vol. 347, no. 1, pp. 116–129, 2010. [Online]. Available: https://www.scopus.com/inward/record.uri?eid=2-s2.0-73649140926&doi=10.1016%2fj.jfranklin.2009.10.013&partnerID=40&md5=4f12493493f705614c92283397f5c0b5
[16] A. L. Schwab and J. P. Meijaard, "How to draw euler angles and utilize euler parameters," ser. International Design Engineering Technical Conferences and Computers and Information in Engineering Conference, vol. Volume 2: 30th Annual Mechanisms and Robotics Conference, Parts A and B, 09 2006, pp. 259–265. [Online]. Available: https://doi.org/10.1115/DETC2006-99307
[17] B. W. Johnson and J. H. Aylor, "Dynamic modeling of an electric wheelchair," *IEEE Transactions on Industry Applications*, vol. IA-21, pp. 1284–1293, 1985. [Online]. Available: https://doi-org.tudelft.idm.oclc.org/10.1109/TIA.1985.349556
[18] R. A. Cooper, "A systems approach to the modeling of racing wheelchair propulsion," *Journal of Rehabilitation Research and Development*, vol. 27, pp. 151–162, 1990. [Online]. Available: https://doi-org.tudelft.idm.oclc.org/10.1682/jrrd.1990.04.0151
[19] C. Sauret, J. Bascou, N. de Saint Remy, H. Pillet, P. Vaslin, and F. Lavaste, "Assessment of field rolling resistance of manual wheelchairs," *Journal of Rehabilitation Research and Development*, vol. 49, pp. 63–74, 2012. [Online]. Available: https://pubmed.ncbi.nlm.nih.gov/22492338/
[20] F. Chenier, P. Bigras, and R. Aissaoui, "An orientation estimator for the wheelchair's caster wheels," *IEEE Transactions on Control Systems Technology*, vol. 19, pp. 1317–1326, 11 2011. [Online]. Available: https://doi-org.tudelft.idm.oclc.org/10.1109/TCST.2010.2084577
[21] J. Bascou, H. Pillet, K. Kollia, C. Sauret, P. Thoreux, and F. Lavaste, "Turning resistance of a manual wheelchair: a theoretical study," *Comput Methods Biomech Biomed Engin*, vol. 17 Suppl 1, pp. 94–95, 2014. [Online]. Available: https://doi-org.tudelft.idm.oclc.org/10.1080/10255842.2014.931159
[22] H. Wang, B. Salatin, G. G. Grindle, D. Ding, and R. A. Cooper, "Real-time model based electrical powered wheelchair control," *Medical Engineering and Physics*, vol. 31, pp. 1244–1254, 12 2009. [Online]. Available: https://doi-org.tudelft.idm.oclc.org/10.1016/j.medengphy.2009.08.002
[23] V. Andaluz, P. Canseco, J. Varela, J. Ortiz, M. Perez, V. Morales, F. Roberti, and R. Carelli, "Modeling and control of a wheelchair considering center of mass lateral displacements," *Lecture Notes in Computer Science (including subseries Lecture Notes in Artificial Intelligence and Lecture Notes in Bioinformatics)*, vol. 9246, pp. 254–270, 2015. [Online]. Available: https://doi-org.tudelft.idm.oclc.org/10.1007/978-3-319-22873-0_23
[24] S. E. Sonenblum, S. Sprigle, and R. A. Lopez, "Manual wheelchair use: Bouts of mobility in everyday life," *Rehabilitation Research and Practice*, vol. 2012, p. 753165, Jul 2012. [Online]. Available: https://doi.org/10.1155/2012/753165
[25] H. Vallery and A. Schwab, *Advanced Dynamics*. Delft University of Technology, 2020.
[26] A. Coolen, R. Kirby, J. Landry, A. MacPhee, D. Dupuis, C. Smith, K. Best, D. MacKenzie, and D. MacLeod, "Wheelchair skills training program for clinicians: A randomized controlled trial with occupational therapy students," *Archives of Physical Medicine and Rehabilitation*, vol. 85, no. 7, pp. 1160–1167, 2004. [Online]. Available: https://www.scopus.com/inward/record.uri?eid=2-s2.0-3242666328&doi=10.1016%2fj.apmr.2003.10.019&partnerID=40&md5=bb91a20ef0bc8647993dae4e7d715fa9
[27] C. De La Cruz, T. Bastos, and R. Carelli, "Adaptive motion control law of a robotic wheelchair," *Control Engineering Practice*, vol. 19, no. 2, pp. 113–125, 2011. [Online]. Available: https://www.scopus.com/inward/record.uri?eid=2-s2.0-78651472331&doi=10.1016%2fj.conengprac.2010.10.004&partnerID=40&md5=9920014d19aeae86ed8fb62d27119860
[28] S. Wang, L. Chen, H. Hu, and K. McDonald-Maier, "Doorway passing of an intelligent wheelchair by dynamically generating bezier curve trajectory," 2012, pp. 1206–1211. [Online]. Available: https://www.scopus.com/inward/record.uri?eid=2-s2.0-84876492784&doi=10.1109%2fROBIO.2012.6491134&partnerID=40&md5=898c11f5066083ab25d010956defdfa3

NOTATION

a	Scalar variable
$\boldsymbol{a}$	Vector
$\hat{\boldsymbol{a}}$	Unit vector
$\ldots^{\mathrm{T}}$	Transpose of a vector or matrix
${}^{\mathcal{N}}\boldsymbol{a}$	Vector expressed in triad $\mathcal{N}$
$\mathbf{A}$	Matrix
$\mathcal{A}$	Triad
$\hat{\boldsymbol{a}}_1$	Unit vector of triad $\mathcal{A}$ in x direction
$\boldsymbol{r}_{A/B}$	Position vector from point A to B
${}^{\mathcal{N}}\mathbf{R}_{\mathcal{A}}$	Rotation matrix from triad $\mathcal{A}$ to triad $\mathcal{N}$ such that ${}^{\mathcal{N}}\boldsymbol{r}_A = {}^{\mathcal{N}}\mathbf{R}_{\mathcal{A}}{}^{\mathcal{A}}\boldsymbol{r}_A$

LIST OF VARIABLES

Design parameters

r_w	Castor wheel radius
r_r	Rear wheel radius
L_{ex}	Castor trail
L_{ey}	Lateral castor trail
L_{df}	Length of swivel axis
σ	Wheel bank angle
ϕ_x	Castor cant angle
ϕ_y	Castor rake angle, also called castor angle or castor stem angle.
a_{f1}	x location of castor connection with respect to vehicle origin
b_{f1}	y location of castor connection with respect to vehicle origin
F_G	Total gravitational force on wheelchair and user combined
m_w	Mass of castor wheel
m_f	Mass of castor fork
m_{wc}	Mass of wheelchair and user excluding the castor wheel

Use variables

r_{turn}	Turn radius of wheelchair
v_{wc}	Forward velocity of wheelchair
F_P	Force applied by user at point P on the push bar
M_P	Moment applied by user at point P on the push bar
P_f	Fraction of weight on the front wheels
P_r	Fraction of weight on the rear wheels
b_P	Lateral location of point P where the wheelchair is pushed

Environment parameters

$f_{\text{r,fi}}$	Roll resistance coefficient of front wheel i
$f_{\text{r,ri}}$	Roll resistance coefficient of rear wheel i
g	Gravity constant

Generalized coordinates

$\boldsymbol{q}$	Generalized coordinate vector
x_B	X position of point B
y_B	Y position of point B
z_B	Z position of point B
ζ_x	Euler angle for X rotation of wheelchair body
ζ_y	Euler angle for Y rotation of wheelchair body
ζ_z	Euler angle for Z rotation of wheelchair body
θ_{ri}	Roll angle of rear wheel i
θ_{fi}	Roll angle of front (castor) wheel i
δ_{fi}	Swivel angle of castor wheel i

Dependent variables

ϵ	Rotation of fork with respect to triad $\mathcal{A}$
γ	Camber angle of wheel with respect to ground plane
η	Heading angle of wheel with respect to inertial triad $\mathcal{N}$
ρ	Steer angle of wheel with respect to body fixed wheelchair triad $\mathcal{B}$

Triads

$\mathcal{N}$	Inertial triad fixed to world
$\mathcal{B}$	Wheelchair body fixed triad
$\mathcal{D}$	Triad fixed to wheelchair with $\hat{\boldsymbol{d}}_3$ in direction of swivel axis
$\mathcal{R}$	Triad rotated with respect to $\mathcal{D}$ around swivel axis
$\mathcal{F}$	Castor fork body fixed triad
$\mathcal{A}$	Triad in direction of contact point from wheel center
$\mathcal{C}$	Triad fixed to contact point
$\mathcal{W}$	Wheel body fixed triad

Important vectors

$\hat{\boldsymbol{n}}$	Normal vector up out of the ground plane
$\hat{\boldsymbol{s}}$	Spin direction of castor wheel
$\hat{\boldsymbol{l}}$	Longitudinal (roll) direction of castor wheel
$\hat{\boldsymbol{t}}$	Transverse direction of castor wheel
$\hat{\boldsymbol{d}}_3$	Swivel axis of castor wheel

APPENDIX A
DESCRIPTION OF KINEMATICS

A. Rotations definitions

In Figure 6c the rotations are shown with the cans in series method. Note that the inertial coordinate system occurs twice since the rotations form a closed loop. To open this closed loop, the angles ϵ, γ, and η are functions of the other angles. The rotation matrices for the free angles are:

$$ {}^{\mathcal{B}}\mathbf{R}_{\mathcal{N}} = \begin{pmatrix} c_{\zeta_z} & s_{\zeta_z} & 0 \\ -s_{\zeta_z} & c_{\zeta_z} & 0 \\ 0 & 0 & 1 \end{pmatrix} \tag{A.1} $$

$$ {}^{\mathcal{D}}\mathbf{R}_{\mathcal{B}} = \begin{pmatrix} 1 & 0 & 0 \\ 0 & c_{\phi_x} & s_{\phi_x} \\ 0 & -s_{\phi_x} & c_{\phi_x} \end{pmatrix} \begin{pmatrix} c_{\phi_y} & 0 & -s_{\phi_y} \\ 0 & 1 & 0 \\ s_{\phi_y} & 0 & c_{\phi_y} \end{pmatrix} \begin{pmatrix} c_{\phi_z} & s_{\phi_z} & 0 \\ -s_{\phi_z} & c_{\phi_z} & 0 \\ 0 & 0 & 1 \end{pmatrix} \tag{A.2} $$

$$ {}^{\mathcal{R}}\mathbf{R}_{\mathcal{D}} = \begin{pmatrix} c_{\delta} & s_{\delta} & 0 \\ -s_{\delta} & c_{\delta} & 0 \\ 0 & 0 & 1 \end{pmatrix} \tag{A.3} $$

$$ {}^{\mathcal{F}}\mathbf{R}_{\mathcal{R}} = \begin{pmatrix} c_{\sigma} & s_{\sigma} & 0 \\ -s_{\sigma} & c_{\sigma} & 0 \\ 0 & 0 & 1 \end{pmatrix} \tag{A.4} $$

$$ {}^{\mathcal{W}}\mathbf{R}_{\mathcal{R}} = \begin{pmatrix} c_{\theta} & 0 & -s_{\theta} \\ 0 & 1 & 0 \\ s_{\theta} & 0 & c_{\theta} \end{pmatrix} \tag{A.5} $$

Rotation matrix ${}^{\mathcal{C}}\mathbf{R}_{\mathcal{F}}$ can be calculated using the unit vectors of triad $\mathcal{C}$:

$$ \hat{\boldsymbol{c}}_1 = \hat{\boldsymbol{l}} \tag{A.6} $$

$$ \hat{\boldsymbol{c}}_2 = \hat{\boldsymbol{t}} \tag{A.7} $$

$$ \hat{\boldsymbol{c}}_3 = -\hat{\boldsymbol{n}} \tag{A.8} $$

A rotation matrix can be written as

$$ {}^{\mathcal{C}}\mathbf{R}_{\mathcal{N}} = \begin{pmatrix} {}^{\mathcal{C}}\hat{\boldsymbol{b}}_1 & {}^{\mathcal{C}}\hat{\boldsymbol{b}}_2 & {}^{\mathcal{C}}\hat{\boldsymbol{b}}_3 \end{pmatrix} = \begin{pmatrix} {}^{\mathcal{B}}\hat{\boldsymbol{c}}_1^{\mathrm{T}} \\ {}^{\mathcal{B}}\hat{\boldsymbol{c}}_2^{\mathrm{T}} \\ {}^{\mathcal{B}}\hat{\boldsymbol{c}}_3^{\mathrm{T}} \end{pmatrix} \tag{A.9} $$

Using this relation and Equations A.11, A.14, and A.13, ${}^{\mathcal{C}}\mathbf{R}_{\mathcal{N}}$ is calculated as

$$ {}^{\mathcal{C}}\mathbf{R}_{\mathcal{B}} = \begin{pmatrix} {}^{\mathcal{B}}\hat{\boldsymbol{l}}^{\mathrm{T}} \\ {}^{\mathcal{B}}\hat{\boldsymbol{t}}^{\mathrm{T}} \\ -{}^{\mathcal{B}}\hat{\boldsymbol{n}}^{\mathrm{T}} \end{pmatrix} \tag{A.10} $$

These directions can be found assuming that ${}^{\mathcal{B}}\mathbf{R}_{\mathcal{F}}$ is known. Vectors $\boldsymbol{n}$ and $\boldsymbol{s}$ are defined by the triad definitions.

$$ {}^{\mathcal{N}}\hat{\boldsymbol{n}} = \begin{pmatrix} 0 \\ 0 \\ -1 \end{pmatrix} \tag{A.11} $$

$$ {}^{\mathcal{F}}\hat{\boldsymbol{s}} = \begin{pmatrix} 0 \\ 1 \\ 0 \end{pmatrix} \tag{A.12} $$

The longitudinal direction vector $\boldsymbol{l}$ is perpendicular to the ground plane and wheel spin vector $\boldsymbol{s}$ for circular wheels. The product is divided by the norm as $\boldsymbol{l}$ and $\boldsymbol{s}$ are not perpendicular.

$$ \hat{\boldsymbol{l}} = \frac{-\hat{\boldsymbol{s}} \times \hat{\boldsymbol{n}}}{\|\hat{\boldsymbol{s}} \times \hat{\boldsymbol{n}}\|} \tag{A.13} $$

The transverse direction $\boldsymbol{t}$ can be determined with a single cross product without dividing by the norm, as both unit vectors are orthogonal by definition.

$$ \hat{\boldsymbol{t}} = \hat{\boldsymbol{l}} \times \hat{\boldsymbol{n}} \tag{A.14} $$

In triad $\mathcal{B}$, these vectors are given by the following expressions.

$$ {}^{\mathcal{B}}\hat{\boldsymbol{n}} = \begin{pmatrix} 0 \\ 0 \\ -1 \end{pmatrix} \tag{A.15} $$

$$ {}^{\mathcal{B}}\hat{\boldsymbol{l}} = \begin{pmatrix} -\frac{\sin(\phi_x)\,\sin(\sigma)-\cos(\delta)\,\cos(\phi_x)\,\cos(\sigma)}{\sqrt{(\cos(\phi_x)\,\sin(\phi_y)\,\sin(\sigma)-\cos(\phi_y)\,\cos(\sigma)\,\sin(\delta)+\cos(\delta)\,\cos(\sigma)\,\sin(\phi_y)\,\sin(\phi_x))^2+(\sin(\phi_x)\,\sin(\sigma)-\cos(\delta)\,\cos(\phi_x)\,\cos(\sigma))^2}} \\ -\frac{\cos(\phi_x)\,\sin(\phi_y)\,\sin(\sigma)-\cos(\phi_y)\,\cos(\sigma)\,\sin(\delta)+\cos(\delta)\,\cos(\sigma)\,\sin(\phi_y)\,\sin(\phi_x)}{\sqrt{(\cos(\phi_x)\,\sin(\phi_y)\,\sin(\sigma)-\cos(\phi_y)\,\cos(\sigma)\,\sin(\delta)+\cos(\delta)\,\cos(\sigma)\,\sin(\phi_y)\,\sin(\phi_x))^2+(\sin(\phi_x)\,\sin(\sigma)-\cos(\delta)\,\cos(\phi_x)\,\cos(\sigma))^2}} \\ 0 \end{pmatrix} \tag{A.16} $$

$$ {}^{\mathcal{B}}\hat{\boldsymbol{t}} = \begin{pmatrix} \frac{\cos(\phi_x)\,\sin(\phi_y)\,\sin(\sigma)-\cos(\phi_y)\,\cos(\sigma)\,\sin(\delta)+\cos(\delta)\,\cos(\sigma)\,\sin(\phi_y)\,\sin(\phi_x)}{\sqrt{(\cos(\phi_x)\,\sin(\phi_y)\,\sin(\sigma)-\cos(\phi_y)\,\cos(\sigma)\,\sin(\delta)+\cos(\delta)\,\cos(\sigma)\,\sin(\phi_y)\,\sin(\phi_x))^2+(\sin(\phi_x)\,\sin(\sigma)-\cos(\delta)\,\cos(\phi_x)\,\cos(\sigma))^2}} \\ -\frac{\sin(\phi_x)\,\sin(\sigma)-\cos(\delta)\,\cos(\phi_x)\,\cos(\sigma)}{\sqrt{(\cos(\phi_x)\,\sin(\phi_y)\,\sin(\sigma)-\cos(\phi_y)\,\cos(\sigma)\,\sin(\delta)+\cos(\delta)\,\cos(\sigma)\,\sin(\phi_y)\,\sin(\phi_x))^2+(\sin(\phi_x)\,\sin(\sigma)-\cos(\delta)\,\cos(\phi_x)\,\cos(\sigma))^2}} \\ 0 \end{pmatrix} \tag{A.17} $$

Using these unit vectors, Equation A.10 can be solved. With this rotation found, all rotations that are relevant to find the equations of motion of the castor wheel have been defined.

B. Positions definitions

The position of the origin of the wheelchair is defined as the point on the symmetry plane coincident with the spin axis of the rear wheels. The X and Y coordinate are described by generalized coordinates x_B and y_B. The height is determined by the radius of the rear wheels, r_r. Recall that the positive Z axis of the inertial coordinate system points into the ground.

$$ {}^{\mathcal{N}}\boldsymbol{r}_{\mathrm{B/O}} = {}^{\mathcal{N}}\,\boldsymbol{r}_{\mathrm{B}} = \begin{pmatrix} x_B \\ y_B \\ -r_r \end{pmatrix} \tag{A.18} $$

Point D is the connection between the wheelchair and the castor wheel. Due to the small angle approximation for the pitch angle of the wheelchair, the Z coordinate of this point is free with respect to point B, and governed by generalized coordinate z_D.

$$ {}^{\mathcal{N}}\boldsymbol{r}_D = \begin{pmatrix} x_B \\ y_B \\ 0 \end{pmatrix} + {}^{\mathcal{N}}\mathbf{R}_{\mathcal{B}} \begin{pmatrix} a_{f1} \\ b_{f1} \\ z_D \end{pmatrix} \tag{A.19} $$

The castor fork contains points F and A.

$$ {}^{\mathcal{N}}\boldsymbol{r}_F = {}^{\mathcal{N}}\boldsymbol{r}_D + {}^{\mathcal{N}}\mathbf{R}_{\mathcal{D}}\,{}^{\mathcal{D}}\boldsymbol{r}_{F/D} = {}^{\mathcal{N}}\boldsymbol{r}_D + {}^{\mathcal{N}}\mathbf{R}_{\mathcal{D}} \begin{pmatrix} 0 \\ 0 \\ L_{df} \end{pmatrix} \tag{A.20} $$

$$ {}^{\mathcal{N}}\boldsymbol{r}_A = {}^{\mathcal{N}}\boldsymbol{r}_F + {}^{\mathcal{N}}\mathbf{R}_{\mathcal{F}}\,{}^{\mathcal{F}}\boldsymbol{r}_{A/F} = {}^{\mathcal{N}}\boldsymbol{r}_D + {}^{\mathcal{N}}\mathbf{R}_{\mathcal{F}} \begin{pmatrix} -L_{ex} \\ L_{ey} \\ 0 \end{pmatrix} \tag{A.21} $$

The direction of point C with respect to point A can be found by taking the cross product of $\hat{\boldsymbol{l}}$ and $\hat{\boldsymbol{s}}$. This can be proven using the fact that

- $\boldsymbol{r}_{C/A}$ lies in the wheel plane $\hat{\boldsymbol{a}}_1$, $\hat{\boldsymbol{a}}_3$
- $\hat{\boldsymbol{l}}$ is tangent to the wheel at point C, and is therefore perpendicular to its radius $\boldsymbol{r}_{C/A}$
- $\hat{\boldsymbol{s}}$ is parallel to $\hat{\boldsymbol{a}}_2$, and thus perpendicular to the wheel plane.

Since $\hat{\boldsymbol{l}}$ and $\hat{\boldsymbol{s}}$ are perpendicular unit vectors, it is not needed to divide by the norm, resulting in:

$$ \hat{\boldsymbol{r}}_{\mathrm{C/A}} = \hat{\boldsymbol{l}} \times \hat{\boldsymbol{s}} \tag{A.22} $$

The contact point C is then defined using the relation found in Equation A.22.

$$ {}^{\mathcal{N}}\boldsymbol{r}_C = {}^{\mathcal{N}}\boldsymbol{r}_A + {}^{\mathcal{N}}\,\hat{\boldsymbol{r}}_{\mathrm{C/A}} \cdot r_w = {}^{\mathcal{N}}\boldsymbol{r}_A + ({}^{\mathcal{N}}\hat{\boldsymbol{l}} \times {}^{\mathcal{N}}\,\hat{\boldsymbol{s}}) \cdot r_w \tag{A.23} $$

Point T is defined as a point that is always fixed to the wheel. This point is mainly used to visualize the rotation of the wheel during simulations.

$$ {}^{\mathcal{N}}\boldsymbol{r}_T = {}^{\mathcal{N}}\boldsymbol{r}_A + {}^{\mathcal{N}}\mathbf{R}_{\mathcal{W}}\,{}^{\mathcal{W}}\boldsymbol{r}_{T/A} = {}^{\mathcal{N}}\boldsymbol{r}_A + {}^{\mathcal{N}}\mathbf{R}_{\mathcal{W}} \begin{pmatrix} 0 \\ 0 \\ r_w \end{pmatrix} \tag{A.24} $$

C. Driven parameters

The camber angle γ and fork pitch angle ϵ can be determined uniquely if ${}^{\mathcal{N}}\mathbf{R}_{\mathcal{F}}$ is known. Recall that the arc cosine is positive definite. To obtain the negative values for γ and ϵ two vectors that are perpendicular in the neutral position can be used. Add or subtract $\pi/2$ to obtain the correct angle. This method is only valid for $[-\pi/2, \pi/2]$, so if a larger range is required a sign operator can be used.

$$\gamma = -\operatorname{acos}(\hat{\boldsymbol{s}} \cdot \hat{\boldsymbol{n}}) + \frac{\pi}{2} \tag{A.25}$$

$$\epsilon = \operatorname{acos}(\hat{\boldsymbol{l}} \cdot \hat{\boldsymbol{f}}_3) - \frac{\pi}{2} \tag{A.26}$$

$$\rho = \operatorname{acos}(\hat{\boldsymbol{l}} \cdot \hat{\boldsymbol{b}}_2) - \frac{\pi}{2} \tag{A.27}$$

The heading angle η between the inertial coordinate system and longitudinal direction vector $\hat{\boldsymbol{l}}$ is equal to

$$\eta = \rho + \zeta_z \tag{A.28}$$

These equations are not used in the calculations, but can become relevant if more tire effects need to be considered.

D. Calculation of (angular) velocities

Velocities are calculated using the partial derivative of the position with respect to the generalized coordinates.

$$\dot{x_i} = \frac{\partial x_i}{\partial q_j}\dot{q_j} \tag{A.29}$$

This equation can be evaluated in vector form by using $\boldsymbol{x}$ containing Cartesian coordinates and the pseudovector $\boldsymbol{q}$ containing all generalized coordinates.

$$\dot{\boldsymbol{x}} = \operatorname{Jacobian}(\boldsymbol{x}, \boldsymbol{q}) \cdot \dot{\boldsymbol{q}} \tag{A.30}$$

The angular velocity can be determined by calculating the tilde matrix of the angular velocity vector. This can be found by multiplying the time derivative of the rotation with the transpose of the rotation matrix [25]. In this calculation ϕ, θ, and ψ are arbitrary Euler angles.

$$\tilde{\boldsymbol{\omega}} = \dot{\mathbf{R}}\mathbf{R}^{\mathrm{T}} \tag{A.31}$$

$$\tilde{\boldsymbol{\omega}} = \frac{\partial \mathbf{R}}{\partial \phi}\mathbf{R}^{\mathrm{T}}\dot{\phi} + \frac{\partial \mathbf{R}}{\partial \theta}\mathbf{R}^{\mathrm{T}}\dot{\theta} + \frac{\partial \mathbf{R}}{\partial \psi}\mathbf{R}^{\mathrm{T}}\dot{\psi} \tag{A.32}$$

This equation can be generalized further when we realize that all Euler angles with nonzero time derivatives must appear in $\boldsymbol{q}$.

$$\tilde{\boldsymbol{\omega}} = \sum_i \frac{\partial \mathbf{R}}{\partial q_i}\mathbf{R}^{\mathrm{T}}\dot{q}_i \tag{A.33}$$

From this tilde matrix the elements of $\boldsymbol{\omega}$ can be read. Notice that all elements are computed twice, this is useful to check the consistency of the solution, but also means that all elements are computed twice.

$$\tilde{\boldsymbol{\omega}} = \begin{pmatrix} 0 & -\omega_z & \omega_y \\ \omega_z & 0 & -\omega_x \\ -\omega_y & \omega_x & 0 \end{pmatrix}, \boldsymbol{\omega} = \begin{pmatrix} \omega_x \\ \omega_y \\ \omega_z \end{pmatrix} \tag{A.34}$$

APPENDIX B
SMALL ANGLE APPROXIMATION FOR LATERAL FORCE ON WHEEL AND STEERING MOMENT

A simpler expression for the moment required to maintain the trajectory can be found by calculating for what reaction forces the moment around the swivel axis equals zero. Recall the following assumptions from section III:
Assumption 15 The weight of the castor wheel is negligible when compared to the weight of the wheelchair and user. Since the castor weight does not accelerate in the Z direction in steady state and has negligible weight, it can be assumed that F_n is equal to the vertical load from the simulation variables, $F_{\mathrm{z,c}}$.
Assumption 13 The wheelchair moves in steady state, which implies that δ does not change over time.

A. Determining the lateral contact force on the castor wheel

Since the swivel axis can rotate freely without any friction, the following equation must hold:

$$M_{\mathrm{D3,D}} = \boldsymbol{M}_D \cdot \hat{\boldsymbol{d}}_3 = 0 \tag{A.35}$$

where

$M_{\mathrm{D3,D}}$is the moment around the swivel axis.
$\boldsymbol{M}_D$ is the moment vector around point D.
$\hat{\boldsymbol{d}}_3$ is the unit vector in the direction of the swivel axis.

The moment around point D can be calculated using the position of point C with respect to D and the reaction forces. The reaction forces at point C, ${}^{\mathcal{C}}\boldsymbol{F}_{\mathrm{C}}$, are expressed in triad C.

$$\boldsymbol{M}_D = \boldsymbol{r}_{C/D} \times \boldsymbol{F}_{\mathrm{C}} \tag{A.36}$$

$${}^{\mathcal{C}}\boldsymbol{F}_{\mathrm{C}} = \begin{pmatrix} F_l \\ F_t \\ -F_n \end{pmatrix} \tag{A.37}$$

To make the dot product of Equation A.35 as simple as possible, the calculations of Equation A.36 can be performed in triad $\mathcal{D}$.

$${}^{\mathcal{D}}\boldsymbol{M}_D = {}^{\mathcal{D}}\boldsymbol{r}_{C/D} \times {}^{\mathcal{D}}\boldsymbol{F}_{\mathrm{C}} = {}^{\mathcal{D}}\mathbf{R}_{\mathcal{N}}{}^{\mathcal{N}}\boldsymbol{r}_{C/D} \times {}^{\mathcal{D}}\mathbf{R}_{\mathcal{C}}{}^{\mathcal{C}}\boldsymbol{F}_{\mathrm{C}} \tag{A.38}$$

In previous research it was shown that small cant angles are sufficient to compensate steering. Therefore Assumption 14(small angle approximation) was made:

$$\sin\phi_y = \phi_y \tag{A.39}$$
$$\cos\phi_y = 1 \tag{A.40}$$
$$\sin\phi_x = \phi_x \tag{A.41}$$
$$\cos\phi_x = 1 \tag{A.42}$$
$$\sin\sigma = \sigma \tag{A.43}$$
$$\cos\sigma = 1 \tag{A.44}$$
$$\tag{A.45}$$

The position vector ${}^{\mathcal{D}}\boldsymbol{r}_{C/D}$ remains a long expression containing many higher order values. It can be split in four parts:

$$\begin{gathered} {}^{\mathcal{D}}\boldsymbol{r}_{C/D} = \begin{pmatrix} -L_{\mathrm{ex}}\cos(\delta) - L_{\mathrm{ey}}\sin(\delta) - A\,C\,r_w\cos(\delta) - A\,B\,r_w\,\sigma\sin(\delta) \\ L_{\mathrm{ey}}\cos(\delta) - L_{\mathrm{ex}}\sin(\delta) - A\,C\,r_w\sin(\delta) + A\,B\,r_w\,\sigma\cos(\delta) \\ L_{\mathrm{df}} + L_{\mathrm{ey}}\,\sigma - A\,B\,r_w \end{pmatrix} \\ A = \frac{1}{\sqrt{B^2 + C^2}} \\ B = \phi_x\,\sigma\cos(\delta) + \phi_y\,\sigma\sin(\delta) - 1 \\ C = \phi_y\cos(\delta) - \phi_x\sin(\delta) \end{gathered} \tag{A.46}$$

Since ϕ_x and ϕ_y both are small terms, a square term is close to zero. Using this assumption the parts of Equation A.46 are simplified as:

$$A = 1 \tag{A.47}$$
$$B = -1 \tag{A.48}$$

The position vector ${}^{\mathcal{D}}\boldsymbol{r}_{C/D}$ can then be written as:

$${}^{\mathcal{D}}\boldsymbol{r}_{C/D} = \begin{pmatrix} r_w\,\sigma\,\sin(\delta) - L_{\mathrm{ey}}\,\sin(\delta) - L_{\mathrm{ex}}\,\cos(\delta) - r_w\,\cos(\delta)\,(\phi_y\,\cos(\delta) - \phi_x\,\sin(\delta)) \\ L_{\mathrm{ey}}\,\cos(\delta) - L_{\mathrm{ex}}\,\sin(\delta) - r_w\,\sigma\,\cos(\delta) - r_w\,\sin(\delta)\,(\phi_y\,\cos(\delta) - \phi_x\,\sin(\delta)) \\ L_{\mathrm{df}} + r_w + L_{\mathrm{ey}}\,\sigma \end{pmatrix} \tag{A.49}$$

The force vector ${}^{\mathcal{D}}\boldsymbol{F}_{\mathrm{C}}$ is with a rotation matrix ${}^{\mathcal{D}}\mathbf{R}_{\mathcal{C}}$ as shown in Equation A.38. This results in

$${}^{\mathcal{D}}\boldsymbol{F}_{\mathrm{C}} = \begin{pmatrix} \phi_y\,F_n + F_l\,\cos(\delta) - F_t\,\sin(\delta) \\ F_t\,\cos(\delta) - \phi_x\,F_n + F_l\,\sin(\delta) + \phi_y\,\phi_x\,(F_l\,\cos(\delta) - F_t\,\sin(\delta)) \\ \phi_y\,(F_l\,\cos(\delta) - F_t\,\sin(\delta)) - F_n - \phi_x\,(F_t\,\cos(\delta) + F_l\,\sin(\delta)) \end{pmatrix} \tag{A.50}$$

In the second row the term $-F_t\,\phi_y\,\phi_x\,\sin(\delta)$ is assumed to be equal to zero as it is much closer to zero than $-\phi_x\,F_n$.

$${}^{\mathcal{D}}\boldsymbol{F}_{\mathrm{C}} = \begin{pmatrix} \phi_y\,F_n + F_l\,\cos(\delta) - F_t\,\sin(\delta) \\ F_t\,\cos(\delta) - \phi_x\,F_n + F_l\,\sin(\delta) \\ \phi_y\,(F_l\,\cos(\delta) - F_t\,\sin(\delta)) - F_n - \phi_x\,(F_t\,\cos(\delta) + F_l\,\sin(\delta)) \end{pmatrix} \tag{A.51}$$

Substituting Equation A.51 and A.49 in Equation A.38 results in a moment of:

$$\begin{gathered} M_{\mathrm{D3,D}} \;=\; \boldsymbol{M}_D \cdot \hat{\boldsymbol{d}}_3 \;=\; ({}^{\mathcal{D}}\boldsymbol{r}_{C/D} \times {}^{\mathcal{D}}\boldsymbol{F}_{\mathrm{C}}) \cdot \hat{\boldsymbol{d}}_3 \;=\; 0 \;= \\ A\,(\phi_y\,F_n + F_l\,\cos(\delta) - F_t\,\sin(\delta)) - B\,(F_t\,\cos(\delta) - \phi_x\,F_n + F_l\,\sin(\delta)) \\ A = L_{\mathrm{ex}}\,\sin(\delta) - L_{\mathrm{ey}}\,\cos(\delta) + r_w\,\sigma\,\cos(\delta) + r_w\,\sin(\delta)\,(\phi_y\,\cos(\delta) - \phi_x\,\sin(\delta)) \\ B = L_{\mathrm{ex}}\,\cos(\delta) + L_{\mathrm{ey}}\,\sin(\delta) - r_w\,\sigma\,\sin(\delta) + r_w\,\cos(\delta)\,(\phi_y\,\cos(\delta) - \phi_x\,\sin(\delta)) \end{gathered} \tag{A.52}$$

This equation can be rewritten explicitly for F_t.

$$\boxed{F_t = \frac{A\,(\phi_y\,F_n + F_l\,\cos(\delta)) + B\,(\phi_x\,F_n - F_l\,\sin(\delta))}{B\,\cos(\delta) + A\,\sin(\delta)}} \tag{A.53}$$

B. Calculating the steering moment by the user

The moment around point B in the Z direction can be found using

$$M_{\mathrm{B3,B}} = (\boldsymbol{r}_{C/B} \times \boldsymbol{F}_{\mathrm{C}}) \cdot \hat{\boldsymbol{b}}_3 = M_{\mathrm{B3,D}} - F_{\mathrm{B1,f1}} b_{\mathrm{f1}} + F_{\mathrm{B1,f2}} a_{\mathrm{f1}} \tag{A.54}$$

$$M_{\mathrm{B3,D}} = (\boldsymbol{r}_{C/D} \times \boldsymbol{F}_{\mathrm{C}}) \cdot \hat{\boldsymbol{b}}_3 \tag{A.55}$$

The force vector on the ground contact point $\boldsymbol{F}_{\mathrm{C}}$ is defined in Equation A.37. Given the small angle approximation of Assumption 14, the rotation ${}^{\mathcal{C}}\mathbf{R}_{\mathcal{B}}$ from Equation A.10 can be simplified.

$$\begin{gathered} {}^{\mathcal{B}}\mathbf{R}_{\mathcal{C}} = {}^{\mathcal{C}}\mathbf{R}_{\mathcal{B}}^{\mathrm{T}} = \begin{pmatrix} B & -A\,\sin(\delta) & 0 \\ A\,\sin(\delta) & B & 0 \\ 0 & 0 & 1 \end{pmatrix}^{\mathrm{T}} = \begin{pmatrix} c_\eta & s_\eta & 0 \\ -s_\eta & c_\eta & 0 \\ 0 & 0 & 1 \end{pmatrix} \\ A = \frac{1}{\sqrt{\sin(\delta)^2 + (\cos(\delta) - \phi_x\,\sigma)^2}} \\ B = A\,(\cos(\delta) - \phi_x\,\sigma) \end{gathered} \tag{A.56}$$

If terms with an order of two and higher for the small angle are omitted, this rotation matrix simply becomes equal to a pure rotation around the $\hat{\boldsymbol{b}}_3$ axis:

$$\begin{gathered} A = 1 \\ B = \cos\delta \\ \Downarrow \\ {}^{\mathcal{B}}\mathbf{R}_{\mathcal{C}} = \begin{pmatrix} \cos(\delta) & -\sin(\delta) & 0 \\ \sin(\delta) & \cos(\delta) & 0 \\ 0 & 0 & 1 \end{pmatrix}^{\mathrm{T}} \end{gathered} \tag{A.57}$$

The reaction force vector $\boldsymbol{F}_{\mathrm{C}}$ is known in triad C as defined in Equation A.37. Using the simplified rotation matrix of Equation A.57, this vector can be described with:

$${}^{\mathcal{B}}\boldsymbol{F}_{\mathrm{C}} = {}^{\mathcal{B}}\mathbf{R}_{\mathcal{C}}\,{}^{\mathcal{C}}\boldsymbol{F}_{\mathrm{C}} = \begin{pmatrix} F_l\,\cos(\delta) - F_t\,\sin(\delta) \\ F_t\,\cos(\delta) + F_l\,\sin(\delta) \\ -F_n \end{pmatrix} \tag{A.58}$$

From this equation the elements of the force vector drawn in Figure 3 can already be derived given the fact that the castor wheel is in steady state. This means that the reaction forces at C are oppsite of those at D.

$$F_{\mathrm{B1,f1}} = F_l \cos(\delta) - F_t \sin(\delta) \tag{A.59}$$

$$F_{\mathrm{B2,f1}} = F_t \cos(\delta) + F_l \sin(\delta) \tag{A.60}$$

The position vector for point C with respect to point B is constructed using

$${}^{\mathcal{B}}\boldsymbol{r}_{C/B} = {}^{\mathcal{B}}\boldsymbol{r}_{C/D} + {}^{\mathcal{B}}\boldsymbol{r}_{D/B} \tag{A.61}$$

$${}^{\mathcal{B}}\boldsymbol{r}_{D/B} = \begin{pmatrix} a_{f1} \\ b_{f1} \\ h_{f1} \end{pmatrix} \tag{A.62}$$

where

a_{f1} is the distance of point D with respect to B in the $\hat{\boldsymbol{b}}_1$ direction.
b_{f1} is the distance of point D with respect to B in the $\hat{\boldsymbol{b}}_2$ direction.
h_{f1} is the distance of point D with respect to B in the $\hat{\boldsymbol{b}}_3$ direction.

The position vector from Equation A.46 can be reused and transformed to the $\mathcal{B}$ triad in Equation A.61. To simplify the equation, all terms that contain a square power or higher of a small angle are omitted.

$${}^{\mathcal{B}}\boldsymbol{r}_{C/D} = {}^{\mathcal{B}}\mathbf{R}_{\mathcal{D}}{}^{\mathcal{D}}\boldsymbol{r}_{C/D} =$$

$$\begin{pmatrix} L_{\mathrm{df}}\,\phi_y + \phi_y\,r_w - L_{\mathrm{ex}}\cos(\delta) - L_{\mathrm{ey}}\sin(\delta) + r_w\,\sigma\sin(\delta) - \phi_y\,r_w\cos(\delta)^2 + \phi_x\,r_w\cos(\delta)\sin(\delta) \\ L_{\mathrm{ey}}\cos(\delta) - L_{\mathrm{df}}\,\phi_x - L_{\mathrm{ex}}\sin(\delta) - r_w\,\sigma\cos(\delta) - \phi_x\,r_w\cos(\delta)^2 - \phi_y\,r_w\cos(\delta)\sin(\delta) \\ L_{\mathrm{df}} + r_w + L_{\mathrm{ey}}\,\sigma + L_{\mathrm{ex}}\,\phi_y\cos(\delta) + L_{\mathrm{ey}}\,\phi_x\cos(\delta) + L_{\mathrm{ey}}\,\phi_y\sin(\delta) - L_{\mathrm{ex}}\,\phi_x\sin(\delta) \end{pmatrix} \tag{A.63}$$

The moment can then be calculated by substituting Equation A.58 and A.63 in A.55, resulting in

$$\boxed{\begin{array}{c} M_{\mathrm{B3,D}} = F_t\,A + F_l\,B \\ A = -L_{\mathrm{ex}} + L_{\mathrm{df}}\,\phi_y\cos(\delta) - L_{\mathrm{df}}\,\phi_x\sin(\delta) \\ B = r_w\,\sigma - L_{\mathrm{ey}} + \phi_x\,r_w\cos(\delta) + \phi_y\,r_w\sin(\delta) + L_{\mathrm{df}}\,\phi_x\cos(\delta) + L_{\mathrm{df}}\,\phi_y\sin(\delta) \end{array}} \tag{A.64}$$

Using Equation A.54 the moment around the vertical wheelchair axis generated by the castor wheel is then calculated as

$$M_{\mathrm{B3,B}} = F_t\,A + F_l\,B - F_{\mathrm{B1,f1}}b_{\mathrm{f1}} + F_{\mathrm{B1,f2}}a_{\mathrm{f1}} \tag{A.65}$$

C. Special cases

If the contribution of the rolling resistance can be omitted either because B or F_l is small, the lateral force is calculated using:

$$\boxed{\begin{array}{c} F_t|_{F_l\,\mathrm{small}} = \dfrac{A\,\phi_y\,F_n + B\,\phi_x\,F_n}{B\cos(\delta) + A\sin(\delta)} \\ A = L_{\mathrm{ex}}\sin(\delta) - L_{\mathrm{ey}}\cos(\delta) + r_w\,\sigma\cos(\delta) + r_w\sin(\delta)\,(\phi_y\cos(\delta) - \phi_x\sin(\delta)) \\ B = L_{\mathrm{ex}}\cos(\delta) + L_{\mathrm{ey}}\sin(\delta) - r_w\,\sigma\sin(\delta) + r_w\cos(\delta)\,(\phi_y\cos(\delta) - \phi_x\sin(\delta)) \end{array}} \tag{A.66}$$

and the moment around point D in the down direction becomes

$$\boxed{M_{\mathrm{B3,D}}|_{F_l\,\mathrm{small}} = F_t\,(-L_{\mathrm{ex}} + L_{\mathrm{df}}\,\phi_y\cos(\delta) - L_{\mathrm{df}}\,\phi_x\sin(\delta))} \tag{A.67}$$

On point B this moment becomes

$$M_{\mathrm{B3,B}}|_{F_l\,\mathrm{small}} = F_t\,(a_{\mathrm{f1}}\cos(\delta) - L_{\mathrm{ex}} + b_{\mathrm{f1}}\sin(\delta) + L_{\mathrm{df}}\,\phi_y\cos(\delta) - L_{\mathrm{df}}\,\phi_x\sin(\delta)) \tag{A.68}$$

If δ is zero, the wheelchair will approximately move in a straight line. The trajectory is not exactly straight since $\hat{\boldsymbol{l}}$ is not exactly parallel to $\boldsymbol{b}_1$ due to ϕ_y as can be seen in Equation A.13. In this special case the equations shorten to:

$$F_t|_{\delta=0} = -\frac{(F_l + \phi_y\,F_n)\,(L_{\mathrm{ey}} - r_w\,\sigma) - \phi_x\,F_n\,(L_{\mathrm{ex}} + \phi_y\,r_w)}{L_{\mathrm{ex}} + \phi_y\,r_w} \tag{A.69}$$

$$M_{\mathrm{B3}}|_{\delta=0} = F_l\,(L_{\mathrm{df}}\,\phi_x - b_{\mathrm{f1}} - L_{\mathrm{ey}} + \phi_x\,r_w + r_w\,\sigma) + F_t\,(a_{\mathrm{f1}} - L_{\mathrm{ex}} + L_{\mathrm{df}}\,\phi_y) \tag{A.70}$$

If in addition to δ, ϕ_y is also zero, the wheelchair does move in a straight line and the equations simplify to:

$$F_t|_{\delta=0\,\wedge\,\phi_y=0} = -\frac{F_l\,(L_{\mathrm{ey}} - r_w\,\sigma) - L_{\mathrm{ex}}\,\phi_x\,F_n}{L_{\mathrm{ex}}} \tag{A.71}$$

$$M_{\mathrm{B3}}|_{\delta=0\,\wedge\,\phi_y=0} = F_l\,(L_{\mathrm{df}}\,\phi_x - b_{\mathrm{f1}} - L_{\mathrm{ey}} + \phi_x\,r_w + r_w\,\sigma) - F_t\,(L_{\mathrm{ex}} - a_{\mathrm{f1}}) \tag{A.72}$$

APPENDIX C
TURNING RADIUS FROM CASTOR SWIVEL ANGLE

The turning radius is defined for this system as the distance between the origin of the body fixed coordinate system B, and the instantaneous center of rotation S. Due to the non-holonomic constraints of the wheels, the tangent vectors $\hat{\boldsymbol{t}}_f$ and $\hat{\boldsymbol{t}}_r$ must intersect at this point. Therefore a radius r_{turn} is defined as the distance between point S and B, and $r_{\mathrm{S,C_f}}$ as the distance between S and C_f.

$$r_{\mathrm{S,C_f}} = -\frac{\hat{\boldsymbol{b}}_1 \cdot \boldsymbol{r}_{C/B}}{\hat{\boldsymbol{b}}_1 \cdot \hat{\boldsymbol{t}}_f} \tag{A.73}$$

$$r_{\mathrm{turn}} = \hat{\boldsymbol{b}}_2 \cdot (\boldsymbol{r}_{C/B} + \hat{\boldsymbol{t}}_f \cdot r_{\mathrm{S,C_f}}) \tag{A.74}$$

Since cant angle ϕ_x and wheel bank angle σ are small and contribute little to the direction of $\hat{\boldsymbol{t}}_f$, the small angle approximation is used. Equation A.39 to A.44 are used here. The vector $\boldsymbol{r}_{C/B}$ was already determined in Equation A.61, substituting this in the above equation and applying the small angle approximations results in:

$$\boxed{r_{\mathrm{turn}} = -\frac{L_{\mathrm{ex}} - a_{\mathrm{f1}}\,\cos(\delta) - b_{\mathrm{f1}}\,\sin(\delta) + L_{\mathrm{df}}\,\phi_x\,\sin(\delta)}{\sin(\delta)}} \tag{A.75}$$

This expression cannot be written explicitly for δ, therefore the small angle approximation is applied to δ as well:

$$r_{\mathrm{turn}}|_{\delta=\mathrm{small}} = -\frac{L_{\mathrm{ex}} - a_{\mathrm{f1}} - b_{\mathrm{f1}}\,\delta + L_{\mathrm{df}}\,\delta\,\phi_x}{\delta} \tag{A.76}$$

$$\delta = -\frac{L_{\mathrm{ex}} - a_{\mathrm{f1}}}{r_{\mathrm{turn}} - b_{\mathrm{f1}} + L_{\mathrm{df}}\,\phi_x} \tag{A.77}$$

Keep in mind that by doing this, the second solution where the wheelchair is moving backwards is lost.

APPENDIX D
DERIVATION OF THE CASTOR GENERALIZED COORDINATES

In subsection II-B it was shown that the generalized coordinates of a wheelchair with one front wheel can be described with the following vector:

$$\boldsymbol{q}_{\mathrm{wc}} = \begin{pmatrix} x_{\mathrm{B}} & y_{\mathrm{B}} & z_{\mathrm{B}} & \zeta_{\mathrm{x}} & \zeta_{\mathrm{y}} & \zeta_{\mathrm{z}} & \theta_{\mathrm{r1}} & \theta_{\mathrm{r2}} & \theta_{\mathrm{f1}} & \delta_{\mathrm{f1}} \end{pmatrix}^{\mathrm{T}} \tag{A.78}$$

Due to the assumption that the ground is flat (Assumption 1) and that the wheels always make contact (Assumption 2), the rear wheels constrain the roll angle and the height of B:

$$\zeta_{\mathrm{x}} = 0 \tag{A.79}$$

$$z_{\mathrm{B}} = -r_{rw} \tag{A.80}$$

The pitch ζ_{y} of conventional wheelchairs is constant as the swivel axis of the castor wheel is perpendicular to the ground plane. However, if this axis is not perpendicular to the ground plane, then the height of point D is a function of δ:

$${}^{\mathcal{N}}\boldsymbol{r}_{D/O} \cdot {}^{\mathcal{N}}\hat{\boldsymbol{n}} = h(\delta) \tag{A.81}$$

If rake angle $\phi_y = 0$, lateral trail $L_{\mathrm{ey}} = 0$, and wheel bank angle $\sigma = 0$, then the height of D with respect to the ground plane simplifies to

$$h(\delta) = L_{\mathrm{df}} \cos(\phi_x) + r_w \sqrt{\cos(\phi_x)^2 + \sin(\delta)^2 \sin(\phi_x)^2} - L_{\mathrm{ex}} \sin(\delta) \sin(\phi_x) \tag{A.82}$$

To find the minimum and maximum value for δ we can take the partial derivative and find its zeros

$$\frac{\partial h(\delta)}{\partial \delta} = \frac{r_w \cos(\delta) \sin(\delta) \sin(\phi_x)^2}{\sqrt{\cos(\phi_x)^2 + \sin(\delta)^2 \sin(\phi_x)^2}} - L_{\mathrm{ex}} \cos(\delta) \sin(\phi_x) \tag{A.83}$$

$$\frac{\partial h(\delta)}{\partial \delta} = 0 \quad \Longleftrightarrow \quad \delta = \pi/2 \quad \vee \quad \delta = -\pi/2 \quad \vee \quad \phi_x = 0 \tag{A.84}$$

In previous research it was determined that a cant angle ϕ_x of approximately 6 degrees provides a moderately strong steering effect. [10] With $a_{\mathrm{f1}} = 0.5\,\mathrm{m}$, $L_{\mathrm{ex}} = 0.1\,\mathrm{m}$ and $L_{\mathrm{ey}} = 0\,\mathrm{m}$ the height can be simplified as:

$$\Delta h_{\max} \quad = \quad |h(\pi/2) - h(-\pi/2)| \quad = \quad 2L_{\mathrm{ex}} \sin\phi_x \quad = \quad 2.09\,\mathrm{cm} \tag{A.85}$$

For $\phi_x = 6^\circ$ this difference results in a pitch angle difference of:

$$\zeta_{\mathrm{y}} = \tan\frac{\Delta h_{\max}}{a_{\mathrm{fi}}} = 2.3^\circ \tag{A.86}$$

This angle is sufficiently small to apply the small angle approximation, and therefore we can assume that (1) the pitch angle ζ_{y} only affects the height of point D, and (2) the height of point D is a linear function of the pitch angle ζ_{y}, and can be substituted by a new variable z_{D}.

Using this assumption a new generalized coordinate vector can be constructed for a single castor wheel. Some generalized coordinates of the wheelchair appear directly in this vector:

$$\boldsymbol{q}_{\mathrm{fi}} = \begin{pmatrix} x_{\mathrm{B}} & y_{\mathrm{B}} & \zeta_{\mathrm{z}} & \theta_{\mathrm{fi}} & \delta_{\mathrm{fi}} & z_{\mathrm{D_{fi}}} \end{pmatrix}^{\mathrm{T}} \tag{A.87}$$

In calculations the fi subscript will be omitted, resulting in the following final vector:

$$\boxed{\boldsymbol{q} = \begin{pmatrix} x_{\mathrm{B}} & y_{\mathrm{B}} & \zeta_{\mathrm{z}} & \theta & \delta & z_{\mathrm{D}} \end{pmatrix}^{\mathrm{T}}} \tag{A.88}$$

APPENDIX E
JUSTIFICATION FOR TOP PROJECTED STEERING CALCULATIONS

A top planar projection is suitable to determine the trajectory of a wheelchair based on input forces and resistances [17], [20], [23], [27], [28]. All of these models assume that the wheel configuration is symmetric. Therefore we have to define a slightly more elaborate model to include the possibility for a modified castor wheel.

A. Sums of forces and moments

The full equilibrium equations can be determined using the free body diagram shown in Figure 3. All forces and moments are drawn in the directions of the B triad, resulting in the following equations:

$$\sum F_{\mathrm{B1}} = F_{\mathrm{B1,f1}} + \sum_{i=1}^{2} F_{\mathrm{B1,ri}} + F_P \tag{A.89}$$

$$\sum F_{\mathrm{B2}} = F_{\mathrm{B2,f1}} + \sum_{i=1}^{2} F_{\mathrm{B2,ri}} \tag{A.90}$$

$$\sum F_{\mathrm{B3}} = F_{\mathrm{B3,f1}} + \sum_{i=1}^{2} F_{\mathrm{B3,ri}} + F_{\mathrm{N3,G}} \tag{A.91}$$

$$\sum M_{\mathrm{B1,G}} = b_{\mathrm{f1}} F_{\mathrm{B3,f1}} + \sum_{i=1}^{2} b_{\mathrm{ri}} F_{\mathrm{B3,ri}} - h_{\mathrm{f1}} F_{\mathrm{B2,f1}} + \sum_{i=1}^{2} r_{w,r} F_{\mathrm{B2,ri}} \tag{A.92}$$

$$\sum M_{\mathrm{B2,G}} = (h_P - h_G)F_P + (h_{\mathrm{f1}} - h_G)F_{\mathrm{B1,f1}} + \sum_{i=1}^{2}(r_{w,r} - h_G)F_{\mathrm{B1,ri}} - (a_{\mathrm{f1}} - a_G)F_{\mathrm{B3,f1}} + \sum_{i=1}^{2} b_{\mathrm{ri}} F_{\mathrm{B3,ri}} \tag{A.93}$$

$$\sum M_{\mathrm{B3,G}} = M_P - b_P F_P + M_{\mathrm{B3,f1}} - b_{\mathrm{f1}} F_{\mathrm{B1,f1}} + (a_{\mathrm{f1}} - a_G)F_{\mathrm{B2,f1}} + \sum_{i=1}^{2} M_{\mathrm{B3,ri}} - \sum_{i=1}^{2} b_{\mathrm{ri}} F_{\mathrm{B1,ri}} \tag{A.94}$$

where

F_{Bj} is a force in direction $\hat{\boldsymbol{b}}_{\mathrm{j}}$.
$M_{\mathrm{Bj,G}}$ is a moment in direction $\hat{\boldsymbol{b}}_{\mathrm{j}}$ calculated around point G.
F_P is the applied force by the user.
$F_{\mathrm{Bj,fi}}$ is a force in direction $\hat{\boldsymbol{b}}_{\mathrm{j}}$ generated by front wheel i.
$F_{\mathrm{Bj,ri}}$ is a force in direction $\hat{\boldsymbol{b}}_{\mathrm{j}}$ generated by rear wheel i.
F_P is the applied force by the user.

If $b_G = 0$, $b_{\mathrm{r1}} = -b_{\mathrm{r2}}$, and $b_{\mathrm{f1}} = 0$, then the moment equations Equation A.92 to A.94 can be simplified. In subsection II-C it is assumed that the wheels have no turn resistance (Assumption 7). Applying these two simplifications results in the following sum of moments:

$$\sum M_{\mathrm{B1,G}} = \sum_{i=1}^{2} b_{\mathrm{ri}} F_{\mathrm{B3,ri}} - (h_{\mathrm{f1}} - h_G)F_{\mathrm{B2,f1}} + \sum_{i=1}^{2} r_{w,r} F_{\mathrm{B2,ri}} \tag{A.95}$$

$$\sum M_{\mathrm{B2,G}} = (h_P - h_G)F_P + (h_{\mathrm{f1}} - h_G)F_{\mathrm{B1,f1}} + \sum_{i=1}^{2}(r_{w,r} - h_G)F_{\mathrm{B1,ri}} - (a_{\mathrm{f1}} - a_G)F_{\mathrm{B3,f1}} \tag{A.96}$$

$$\sum M_{\mathrm{B3,G}} = M_P - b_P F_P + M_{\mathrm{B3,f1}} + (a_{\mathrm{f1}} - a_G)F_{\mathrm{B2,f1}} - \sum_{i=1}^{2} b_{\mathrm{ri}} F_{\mathrm{B1,ri}} \tag{A.97}$$

If the contributions of lateral forces are assumed small in comparison to the normal forces, only the normal forces on the rear wheels contribute to the moment equilibrium around the forward axis:

$$\sum M_{\mathrm{B1,G}} = b_{\mathrm{r1}}(F_{\mathrm{B3,r1}} - F_{\mathrm{B3,r2}}) \tag{A.98}$$

which means that the normal forces on the rear wheels are equal for a symmetric wheelchair moving at low velocities. Since roll resistance is proportional to normal force, Assumption 5 states that the roll resistance of both rear wheels is equal.

The rolling resistance of the wheels is calculated using the coefficient of rolling resistance $f_{r,f}$ and $f_{r,r}$ for the front and rear wheels respectively. The force is calculated as

$$F_{\mathrm{B1,ri}} = \mathrm{sgn}\,(\dot{\theta}_{\mathrm{ri}}) F_{\mathrm{B3,ri}} f_{r,r} \tag{A.99}$$

$$F_{\mathrm{l,f1}} = \mathrm{sgn}\,(\dot{\theta}_{\mathrm{f1}}) F_{\mathrm{B3,f1}} f_{r,f} \tag{A.100}$$

In Appendix B it was shown that $F_{\mathrm{t,f1}}$ is also a function of the vertical load $F_{\mathrm{B3,f1}}$. Since the rolling resistance (and therefore the pushing force F_P) is a function of vertical load as well, the moment equation along the lateral wheelchair axis can be split in a part that is dependent on the vertical load on the front and rear wheels.

$$\sum M_{\mathrm{B2,G}} = C_{\mathrm{f}} F_{\mathrm{B3,f1}} + C_{\mathrm{r}} \sum_{i=1}^{2} F_{\mathrm{B3,ri}} = 0 \tag{A.101}$$

where

C_{f} is a constant such that $C_{\mathrm{f}} F_{\mathrm{B3,f1}}$ is equal to the contributions to Equation A.93 that linearly depend on $F_{\mathrm{B3,f1}}$.

C_{r} is a constant such that $C_{\mathrm{r}} \sum_{i=1}^{2} F_{\mathrm{B3,ri}}$ is equal to the contributions to Equation A.93 that linearly depend on $\sum_{i=1}^{2} F_{\mathrm{B3,ri}}$.

Using the vertical equilibrium equation A.91, the vertical force of gravity on the wheelchair $F_{\mathrm{N3,G}}$ must equal the combined normal forces of the wheels:

$$F_{\mathrm{N3,G}} = -F_{\mathrm{B3,f1}} - \sum_{i=1}^{2} F_{\mathrm{B3,ri}} \tag{A.102}$$

To achieve a certain weight distribution between the front and the rear wheels, the location of the center of mass can be shifted. If the center of mass G is fully above the rear wheels ($a_G = 0$) then all weight is on the rear wheels. If the center is all the way to the front instead ($a_G = a_{\mathrm{f1}}$), then all weight is on the front wheels.

$$a_G = -C_{\mathrm{f}} \frac{F_{\mathrm{B3,f1}}}{F_{\mathrm{B3,f1}} + \sum_{i=1}^{2} F_{\mathrm{B3,ri}}} - C_{\mathrm{r}} \frac{\sum_{i=1}^{2} F_{\mathrm{B3,ri}}}{F_{\mathrm{B3,f1}} + \sum_{i=1}^{2} F_{\mathrm{B3,ri}}} \tag{A.103}$$

These fractions represent the part of the weight that is supported by the front or by the rear wheels, and is defined as

$$\begin{aligned} P_f &= \frac{F_{\mathrm{B3,f1}}}{F_{\mathrm{B3,f1}} + \sum_{i=1}^{2} F_{\mathrm{B3,ri}}} \\ P_r &= \frac{\sum_{i=1}^{2} F_{\mathrm{B3,ri}}}{F_{\mathrm{B3,f1}} + \sum_{i=1}^{2} F_{\mathrm{B3,ri}}} \end{aligned} \tag{A.104}$$

This leads to Assumption 9: weight distribution is constant and can be expressed using a fraction. The forces $F_{\mathrm{B3,ri}}$ and $F_{\mathrm{B3,f1}}$ then are constant and expressed as:

$$F_{\mathrm{B3,f1}} = m_{\mathrm{wc}} g P_f \tag{A.105}$$

$$F_{\mathrm{B3,ri}} = m_{\mathrm{wc}} g \frac{P_r}{2} \tag{A.106}$$

where

P_f is the fraction of the weight that is supported by the front wheels.

P_r is the fraction of the weight that is supported by the rear wheels.

g is the gravity constant of $9.81\,\mathrm{m/s^2}$.

m_{wc} is the total weight of the wheelchair and user.

Since the weight distribution is constant, the rolling resistances are constant as well. The total rolling resistance of the front and rear wheels can be calculated as

$$F_{\mathrm{B1,ri}} = \mathrm{sgn}\,(\dot{\theta}_{\mathrm{ri}}) F_{\mathrm{B3,ri}} f_{r,r} = \mathrm{sgn}\,(\dot{\theta}_{\mathrm{ri}}) m_{\mathrm{wc}} g P_f f_{r,r} \tag{A.107}$$

$$F_{\mathrm{l,f1}} = \mathrm{sgn}\,(\dot{\theta}_{\mathrm{f1}}) F_{\mathrm{B3,f1}} f_{r,f} = \mathrm{sgn}\,(\dot{\theta}_{\mathrm{f1}}) m_{\mathrm{wc}} g \frac{P_r}{2} f_{r,f} \tag{A.108}$$

Combining the above results, the movement of the wheelchair can be described using only three equilibrium equations, which can be simplified to:

$$\sum F_{\mathrm{B1}} = F_{\mathrm{B1,f1}} + \sum_{i=1}^{2} F_{\mathrm{B1,ri}} + F_{\mathrm{P}} \tag{A.109}$$

$$\sum F_{\mathrm{B2}} = F_{\mathrm{B2,f1}} + \sum_{i=1}^{2} F_{\mathrm{B2,ri}} \tag{A.110}$$

$$\sum M_{\mathrm{B3,G}} = M_{\mathrm{P}} - b_P F_P + M_{\mathrm{B3,D}} - b_{\mathrm{f1}} F_{\mathrm{B1,D}} + (a_{\mathrm{f1}} - a_G) F_{\mathrm{B2,D}} - \sum_{i=1}^{2} a_G F_{\mathrm{B2,ri}} \tag{A.111}$$

APPENDIX F
DERIVATION OF EQUATIONS OF MOTION USING LAGRANGE AND TMT METHOD

In section IV the constraint equations and assumptions are defined. In this section the Lagrange and TMT method are used to write the equations of motion in the form

$$\begin{pmatrix} \bar{\mathbf{M}} & \mathbf{C}_q^{\mathrm{T}} \\ \mathbf{C}_q & \mathbf{0} \end{pmatrix} \begin{pmatrix} \ddot{\boldsymbol{q}} \\ \boldsymbol{\lambda} \end{pmatrix} = \begin{pmatrix} \boldsymbol{f} \\ \mathbf{C}_{qq}\dot{\boldsymbol{q}} \end{pmatrix} \tag{A.112}$$

where

$\bar{\mathbf{M}}$ is the generalized mass matrix
$\mathbf{C}_q$ is the Jacobian matrix of constraints
$\mathbf{0}$ is a zero matrix
$\boldsymbol{\lambda}$ is the vector of Lagrange multipliers for each constraint
$\boldsymbol{f}$ is the vector with generalized forces
$\mathbf{C}_{qq}$ is the Jacobian matrix of $\mathbf{C_q}\dot{\boldsymbol{q}}$ over $\boldsymbol{q}$, which includes the terms that do not depend on the accelerations.

All terms except $\bar{\mathbf{M}}$ and $\boldsymbol{f}$ are the same for both the Lagrange and TMT method. The Jacobian of the constraints $\mathbf{C}_q$ and $\mathbf{C}_{qq}$ were defined in Equation A.119 and Equation A.121 respectively.

A. Kinematic constraints and their derivatives

The constraint equations from section IV can be split between holonomic and nonholonomic constraints. The constraint vector $\boldsymbol{C}_{\mathrm{h}}$ is defined for holonomic constraints, and $\boldsymbol{C}_{\mathrm{nh}}$ for nonholonomic constraints:

$$\boldsymbol{C}_{\mathrm{h}} = \left(C_{\mathrm{C\_normal}}\right) = \mathbf{0} \tag{A.113}$$

$$\boldsymbol{C}_{\mathrm{nh}} = \begin{pmatrix} C_{\mathrm{C\_longitudinal}} \\ C_{\mathrm{C\_tangent}} \\ C_{\mathrm{B\_tangent}} \\ C_{\mathrm{B\_fixed\_velocity}} \\ C_{\mathrm{B\_fixed\_rotation}} \end{pmatrix} = \mathbf{0} \tag{A.114}$$

The time derivatives of these vectors can be calculated using

$$\dot{\boldsymbol{C}}_{\mathrm{h}} = \mathrm{Jacobian}(\boldsymbol{C}_{\mathrm{h}}, \boldsymbol{q}) \cdot \dot{\boldsymbol{q}} = \mathbf{0} \tag{A.115}$$

$$\dot{\boldsymbol{C}}_{\mathrm{nh}} = \mathrm{Jacobian}(\boldsymbol{C}_{\mathrm{nh}}, \dot{\boldsymbol{q}}) \cdot \dot{\boldsymbol{q}} = \mathbf{0} \tag{A.116}$$

The Jacobian is defined as

$$\mathrm{Jacobian}(\boldsymbol{a}, \boldsymbol{q}) = \begin{pmatrix} \frac{\partial a_1}{\partial q_1} & \cdots & \frac{\partial a_1}{\partial q_n} \\ \vdots & \ddots & \vdots \\ \frac{\partial a_n}{\partial q_1} & \cdots & \frac{\partial a_n}{\partial q_n} \end{pmatrix} \tag{A.117}$$

These equations can be combined using

$$\mathbf{C}_q = \begin{pmatrix} \mathrm{Jacobian}(\boldsymbol{C}_{\mathrm{h}}, \boldsymbol{q}) \\ \mathrm{Jacobian}(\boldsymbol{C}_{\mathrm{nh}}, \dot{\boldsymbol{q}}) \end{pmatrix} \tag{A.118}$$

$$\mathbf{C}_q \cdot \dot{\boldsymbol{q}} = \mathbf{0} \tag{A.119}$$

Since the equation of motion are solved using $\ddot{\boldsymbol{q}}$, this equation has to be differentiated with respect to time once more:

$$\mathbf{C}_q \cdot \ddot{\boldsymbol{q}} + \mathbf{C}_{qq} \cdot \dot{\boldsymbol{q}} = \mathbf{0} \tag{A.120}$$

where

$$\mathbf{C}_{qq} = \mathrm{Jacobian}(\mathbf{C}_q \cdot \dot{\boldsymbol{q}}, \boldsymbol{q}) \tag{A.121}$$

B. Generalized forces

The generalized forces are calculated as:

$$\boldsymbol{Q} = \sum \boldsymbol{F}_i \cdot \frac{\partial \boldsymbol{r}_i}{\partial \boldsymbol{q}} \tag{A.122}$$

where

$\boldsymbol{Q}$ is the generalized force pseudovector. Each element Q_j corresponds to q_j.
$\boldsymbol{F}_i$ is a force vector i in Cartesian space.
$\boldsymbol{r}_i$ is the application point of the considered force vector i.

All conservative forces are inlcuded in $\boldsymbol{Q}_{\mathrm{c}}$, and all other forces, including forces which might be conservative, are included in $\boldsymbol{Q}_{\mathrm{nc}}$.

C. Lagrange

The kinetic energy for any body can be found using the linear and angular velocity in the inertial coordinate system $\mathcal{N}$. The derivation for these is given in Appendix A. The kinetic energy of a body i is then equal to:

$$T_i = \frac{1}{2} m_i \dot{\boldsymbol{r}}_{G_i/O}^{\mathrm{T}} \cdot \dot{\boldsymbol{r}}_{G_i/O} + \frac{1}{2} \boldsymbol{\omega}_{\mathcal{B}/\mathcal{N}}^{\mathrm{T}} \cdot \mathbf{I}_{\mathrm{i,G_i}} \cdot \boldsymbol{\omega}_{\mathcal{B}/\mathcal{N}} \tag{A.123}$$

where

m_i is the mass of body i.
O is the origin of the inertial coordinate system.
G_i is the center of mass of body i.
$\mathcal{B}$ is the body fixed triad of body i.
$\mathbf{I}_{\mathrm{i,G_i}}$ is the mass moment of inertia tensor of body i around its center of mass G_i.
$\boldsymbol{\omega}_{\mathcal{B}/\mathcal{N}}$ is the angular velocity of body i with respect to $\mathcal{N}$.

For potential energy only conservative forces contribute. Therefore it can be written as

$$V_i = -\boldsymbol{r}_{ci} \cdot \boldsymbol{F}_{ci} \tag{A.124}$$

Since gravity is the only conservative force in this system, the potential energy for each body i can be written as

$$V_i = -m_i \, g \, \boldsymbol{r}_{G_i/O} \cdot \hat{\boldsymbol{n}}_3 \tag{A.125}$$

where

$\boldsymbol{r}_{G_i/O}$ is the location of the center of mass of body i.
$\hat{\boldsymbol{n}}_3$ is the down direction of the inertial coordinate system.

The wheelchair is considered to be driving on a flat surface, $\hat{\boldsymbol{n}}3$ is equal to $-\hat{\boldsymbol{n}}$. The Lagrangian of the system is equal to

$$\mathcal{L} = \sum (T_i - V_i) \tag{A.126}$$

The Lagrange's equation can be used to find the equations of motion using the Lagrangian. Each generalized coordinate q_j will yield the following equation:

$$\frac{\mathrm{d}}{\mathrm{d}t}\left(\frac{\partial \mathcal{L}}{\partial \dot{q}_j}\right) - \frac{\partial \mathcal{L}}{\partial q_j} = Q_j + \sum \lambda a_{ij} \tag{A.127}$$

When written in vector form this equation is calculated as

$$\frac{\mathrm{d}}{\mathrm{d}t}\left(\frac{\partial \mathcal{L}}{\partial \dot{\boldsymbol{q}}}\right) - \frac{\partial \mathcal{L}}{\partial \boldsymbol{q}} = \boldsymbol{Q}_{\mathrm{nc}} + \mathbf{C}_q \boldsymbol{\lambda} \tag{A.128}$$

The (partial) derivatives of the Lagrangian are calculated using the following equations:

$$\frac{\partial \mathcal{L}}{\partial \boldsymbol{q}} = \mathrm{Jacobian}(\mathcal{L}, \boldsymbol{q}) = \nabla^{\mathrm{T}} \mathcal{L}(\boldsymbol{q}) \tag{A.129}$$

$$\frac{\partial \mathcal{L}}{\partial \dot{\boldsymbol{q}}} = \mathrm{Jacobian}(\mathcal{L}, \dot{\boldsymbol{q}}) = \nabla^{\mathrm{T}} \mathcal{L}(\dot{\boldsymbol{q}}) \tag{A.130}$$

$$\frac{\mathrm{d}}{\mathrm{d}t}\left(\frac{\partial \mathcal{L}}{\partial \dot{\boldsymbol{q}}}\right) = \mathrm{Jacobian}\left(\frac{\partial \mathcal{L}}{\partial \dot{\boldsymbol{q}}}, \boldsymbol{q}\right) \dot{\boldsymbol{q}} + \mathrm{Jacobian}\left(\frac{\partial \mathcal{L}}{\partial \dot{\boldsymbol{q}}}, \dot{\boldsymbol{q}}\right) \ddot{\boldsymbol{q}} \tag{A.131}$$

These expressions are used to write Equation A.128 and the constraint equations in the form of Equation A.112:

$$\bar{\mathbf{M}} = \mathrm{Jacobian}\left(\frac{\partial \mathcal{L}}{\partial \dot{\boldsymbol{q}}}, \dot{\boldsymbol{q}}\right) \tag{A.132}$$

$$\boldsymbol{f} = \boldsymbol{Q}_{\mathrm{nc}} + \frac{\partial \mathcal{L}}{\partial \boldsymbol{q}} - \mathrm{Jacobian}\left(\frac{\partial \mathcal{L}}{\partial \dot{\boldsymbol{q}}}, \boldsymbol{q}\right) \dot{\boldsymbol{q}} \tag{A.133}$$

resulting in the system

$$\boxed{\begin{pmatrix} \mathrm{Jacobian}\left(\frac{\partial \mathcal{L}}{\partial \dot{\boldsymbol{q}}}, \dot{\boldsymbol{q}}\right) & \mathbf{C}_q^{\mathrm{T}} \\ \mathbf{C}_q & \mathbf{0} \end{pmatrix} \begin{pmatrix} \ddot{\boldsymbol{q}} \\ \boldsymbol{\lambda} \end{pmatrix} = \begin{pmatrix} \boldsymbol{Q}_{\mathrm{nc}} + \frac{\partial \mathcal{L}}{\partial \boldsymbol{q}} - \mathrm{Jacobian}\left(\frac{\partial \mathcal{L}}{\partial \dot{\boldsymbol{q}}}, \boldsymbol{q}\right) \dot{\boldsymbol{q}} \\ \mathbf{C}_{qq} \dot{\boldsymbol{q}} \end{pmatrix}} \tag{A.134}$$

D. TMT

The TMT method [25] uses virtual power as a function of the pose of each body i to derive the equation of motion. The pose contains the Cartesian coordinates of the center of mass and the Euler angles to reach its orientation with respect to the inertial coordinate system $\mathcal{N}$. The virtual power can then be written as

$$\delta P_i = \delta \dot{\boldsymbol{x}}_i^{\mathrm{T}} (\boldsymbol{F}_i - \mathbf{M}_i \ddot{\boldsymbol{x}}_i) \tag{A.135}$$

where

- δP_i is the virtual power
- $\boldsymbol{x}_i$ is the pose of body i
- $\delta \dot{\boldsymbol{x}}_i$ are the virtual velocities
- $\boldsymbol{F}_i$ are all external forces and moments on body i, decomposed in the directions of $\boldsymbol{x}_i$.
- $\mathbf{M}_i$ is the mass matrix for body i, where the masses and mass moment of inertia terms are written on the diagonal

To calculate the sum of the virtual power of the entire system can be written in a similar form. The vectors $\boldsymbol{x}$ and $\boldsymbol{F}$ are built combining the vectors from Equation A.135

$$\boldsymbol{x} = \begin{pmatrix} \boldsymbol{x}_1^{\mathrm{T}} & \boldsymbol{x}_2^{\mathrm{T}} & \dots & \boldsymbol{x}_n^{\mathrm{T}} \end{pmatrix}^{\mathrm{T}} \tag{A.136}$$

$$\boldsymbol{F} = \begin{pmatrix} \boldsymbol{F}_1^{\mathrm{T}} & \boldsymbol{F}_2^{\mathrm{T}} & \dots & \boldsymbol{F}_n^{\mathrm{T}} \end{pmatrix}^{\mathrm{T}} \tag{A.137}$$

and the mass matrix $\mathbf{M}$ can be written as

$$\mathbf{M} = \begin{pmatrix} \mathbf{M}_1 & \mathbf{0} & \dots & \mathbf{0} \\ \mathbf{0} & \mathbf{M}_1 & \dots & \mathbf{0} \\ \vdots & \vdots & \ddots & \\ \mathbf{0} & \mathbf{0} & & \mathbf{M}_n \end{pmatrix} \tag{A.138}$$

The virtual velocities can also be written as a function of the generalized coordinates. The vector $\boldsymbol{T}$ is defined such that

$$\boldsymbol{x} = \boldsymbol{T}(\boldsymbol{q}) \tag{A.139}$$

The velocities and accelerations are then equal to

$$\dot{\boldsymbol{x}} = \mathbf{T}_q \dot{\boldsymbol{q}} \tag{A.140}$$

$$\ddot{\boldsymbol{x}} = \mathbf{T}_q \ddot{\boldsymbol{q}} + \mathbf{T}_{qq} \dot{\boldsymbol{q}} \tag{A.141}$$

where

$$\mathbf{T}_q = \mathrm{Jacobian}(\boldsymbol{T}, \boldsymbol{q}) \tag{A.142}$$

$$\mathbf{T}_{qq} = \mathrm{Jacobian}(\mathbf{T}_q \dot{\boldsymbol{q}}, \boldsymbol{q}) \tag{A.143}$$

The virtual power in terms of the generalized coordinates is given by

$$\delta P = \delta(\mathbf{T}_q \dot{\boldsymbol{q}})^{\mathrm{T}} (\boldsymbol{F} - \mathbf{M}(\mathbf{T}_q \ddot{\boldsymbol{q}} + \mathbf{T}_{qq} \dot{\boldsymbol{q}})) \tag{A.144}$$

The system is in equilibrium if and only if the sum of the virtual powers for all bodies of the system is zero for all virtual velocities which do not violate the kinematic constraints.

$$\text{System in equilibrium} \iff \sum_{i=0}^{n} \delta P_i = 0 \; \forall \; \delta \dot{\boldsymbol{x}} \tag{A.145}$$

To solve this equation, $\delta \dot{\boldsymbol{x}}$ should be chosen such that the virtual velocity does not point in a constrained direction. By definition, the derivative of $\boldsymbol{T}$ over $\boldsymbol{q}$ must point in a direction that is kinematically admissible.

$$\delta \dot{\boldsymbol{x}} = \mathbf{T}_q \delta \dot{\boldsymbol{q}} \tag{A.146}$$

always satisfy the kinematic constraints if all the generalized coordinates q_j are independent in velocity space. If extra constraints are imposed on the generalized coordinates, an extra term with Lagrange multipliers must be included. These additional constraints are defined in section IV, and lead to a term similar to Equation A.128. The sum of virtual power in Equation A.144 can be rewritten to contain terms dependent on $\ddot{\boldsymbol{q}}$ and $\boldsymbol{\lambda}$ on the left, and the rest on the right.

$$\mathbf{T}_q^{\mathrm{T}} (\boldsymbol{F} - \mathbf{M}(\mathbf{T}_q \ddot{\boldsymbol{q}} + \mathbf{T}_{qq} \dot{\boldsymbol{q}})) = \mathbf{C}_q^{\mathrm{T}} \boldsymbol{\lambda} \tag{A.147}$$

$$\mathbf{T}_q^{\mathrm{T}} \boldsymbol{F} - \mathbf{T}_q^{\mathrm{T}} \mathbf{M} \mathbf{T}_q \ddot{\boldsymbol{q}} + \mathbf{T}_q^{\mathrm{T}} \mathbf{M} \mathbf{T}_{qq} \dot{\boldsymbol{q}} = \mathbf{C}_q^{\mathrm{T}} \boldsymbol{\lambda} \tag{A.148}$$

$$\mathbf{T}_q^{\mathrm{T}} \mathbf{M} \mathbf{T}_q \ddot{\boldsymbol{q}} + \mathbf{C}_q^{\mathrm{T}} \boldsymbol{\lambda} = \mathbf{T}_q^{\mathrm{T}} \boldsymbol{F} + \mathbf{T}_q^{\mathrm{T}} \mathbf{M} \mathbf{T}_{qq} \dot{\boldsymbol{q}} \tag{A.149}$$

The additional constraint equations described in Equation A.120 must also be satisfied, so

$$\mathbf{C}_q \cdot \ddot{\boldsymbol{q}} = -\mathbf{C}_{qq} \cdot \dot{\boldsymbol{q}} \tag{A.150}$$

These equations can be written in the form of Equation A.112 as

$$\boxed{\begin{pmatrix} \mathbf{T}_q^{\mathrm{T}}\mathbf{M}\mathbf{T}_q & \mathbf{C}_q^{\mathrm{T}} \\ \mathbf{C}_q & \mathbf{0} \end{pmatrix} \begin{pmatrix} \ddot{\boldsymbol{q}} \\ \boldsymbol{\lambda} \end{pmatrix} = \begin{pmatrix} \mathbf{T}_q^{\mathrm{T}}\boldsymbol{F} + \mathbf{T}_q^{\mathrm{T}}\mathbf{M}\mathbf{T}_{qq}\dot{\boldsymbol{q}} \\ \mathbf{C}_{qq}\dot{\boldsymbol{q}} \end{pmatrix}} \tag{A.151}$$

It is worth noting that the term $\mathbf{T}_q^{\mathrm{T}}\boldsymbol{F}$ is equal to $\boldsymbol{Q}$ as defined in Equation A.122, if both conservative and nonconservative forces are included.

E. Constraint projection for the initial state

An estimate of the state is chosen as

$$\bar{\boldsymbol{Y}} = \begin{pmatrix} \bar{\boldsymbol{q}} \\ \bar{\dot{\boldsymbol{q}}} \end{pmatrix} \tag{A.152}$$

and the error on the state is defined in configuration space as

$$\boldsymbol{Y} = \bar{\boldsymbol{Y}} + \Delta\boldsymbol{Y} \tag{A.153}$$

where

$\boldsymbol{Y}$ is the true positions where the kinematic constraints are satisfied
$\bar{\boldsymbol{Y}}$ is the estimate of the positions
$\Delta\boldsymbol{Y}$ is the error between the true and estimate positions

This equation can be considered separately for the positions and velocities.

$$\boldsymbol{q} = \bar{\boldsymbol{q}} + \Delta\boldsymbol{q} \tag{A.154}$$

$$\dot{\boldsymbol{q}} = \bar{\dot{\boldsymbol{q}}} + \Delta\dot{\boldsymbol{q}} \tag{A.155}$$

Since there are multiple degrees of freedom in configuration space, there is an infinite number of feasible positions $\boldsymbol{q}$ on the constraint surface. The true position is defined as the closest valid position relative to the estimated position $\bar{\boldsymbol{q}}$ in configuration space. The estimated position does not have to lie on the constraint surface, as if it did the true and estimate position are equal. For a system with only linear constraints, the smallest distance between the true and estimated position is calculated as [25]

$$\Delta\boldsymbol{q} = \mathbf{C}_q^{\mathrm{T}}(\mathbf{C}_q\mathbf{C}_q^{\mathrm{T}})^{-1} \tag{A.156}$$

Since the only holonomic constraint (Equation 39) of this system is not linear, the coordinate projection has to be applied iteratively. The equation

$$\bar{\boldsymbol{q}} = \bar{\boldsymbol{q}} - \mathbf{C}_q^{\mathrm{T}}(\mathbf{C}_q\mathbf{C}_q^{\mathrm{T}})^{-1}\boldsymbol{C} \tag{A.157}$$

is applied until $\bar{\boldsymbol{q}} = \boldsymbol{q}$, which is approximately true if the violation of the constraints $\boldsymbol{C}(\bar{\boldsymbol{q}})$ approaches the zero vector.

The velocities can be projected using a similar method. Since the nonholonimic constraint equations are linear in velocity space, this projection can be applied in a single step

$$\Delta\dot{\boldsymbol{q}} = \mathbf{C}_q^{\mathrm{T}}(\mathbf{C}_q\mathbf{C}_q^{\mathrm{T}})^{-1}\dot{\boldsymbol{C}} \tag{A.158}$$

where

$$\dot{\boldsymbol{C}} = \mathbf{C}_q\dot{\boldsymbol{q}} \tag{A.159}$$

resulting in

$$\dot{\boldsymbol{q}} = \bar{\dot{\boldsymbol{q}}} - \mathbf{C}_q^{\mathrm{T}}(\mathbf{C}_q\mathbf{C}_q^{\mathrm{T}})^{-1}\dot{\boldsymbol{C}} \tag{A.160}$$

For the chosen constraints, the number of degrees of freedom in velocity space is zero. This means that there is only one feasible $\dot{\boldsymbol{q}}$, regardless of the choice of $\bar{\dot{\boldsymbol{q}}}$.